Interannual variability in glacier contribution to runoff from a high-elevation Andean catchment: understanding the role of debris cover in glacier hydrology.

Flavia Burger[1], Alvaro Ayala[2,3], David Farias[4], Thomas E. Shaw[5], Shelley MacDonell[6], Ben Brock[1], James McPhee[5,7], Francesca Pellicciotti[1,3]

[1]Northumbria University, Department of Geography and Environmental Sciences, Newcastle upon Tyne, United Kingdom

[2]Laboratory of Hydraulics, Hydrology and Glaciology (VAW), ETH Zurich, Zurich Switzerland

[3]Swiss Federal Institute for Forest, Snow and Landscape research WSL, Birmensdorf, Switzerland

[4]Institute of Geography and Geosciences, Friedrich-Alexander-University Erlangen-Nürnberg (FAU), Erlangen, Germany

[5]Advanced Mining Technology Center, Universidad de Chile, Santiago, Chile

[6]Centro de Estudios Avanzados en Zonas Aridas (CEAZA), La Serena, Chile

[7]Department of Civil Engineering, Faculty of Physical and Mathematical Science, Universidad de Chile, Santiago, Chile

Corresponding author: Flavia Burger, flaviburger@gmail.com

This article has been accepted for publication and undergone full peer review but has not been through the copyediting, typesetting, pagination and proofreading process which may lead to differences between this version and the Version of Record. Please cite this article as doi: 10.1002/hyp.13354

Abstract:

We present a field-data rich modelling analysis to reconstruct the climatic forcing, glacier response and runoff generation from a high elevation catchment in central Chile over the period 2000-2015, to provide insights into the differing contributions of debris-covered and debris-free glaciers under current and future changing climatic conditions. Model simulations with the physically-based glacio-hydrological model TOPKAPI-ETH reveal a period of neutral or slightly positive mass balance between 2000-2010, followed by a transition to increasingly large annual mass losses, associated with a recent mega drought. Mass losses commence earlier, and are more severe, for a heavily debris-covered glacier, most likely due to its strong dependence on snow avalanche accumulation, which has declined in recent years. Catchment runoff shows a marked decreasing trend over the study period, but with high interannual variability directly linked to winter snow accumulation, and high contribution from ice melt in dry periods and drought conditions. The study demonstrates the importance of incorporating local-scale processes such as snow avalanche accumulation and spatially variable debris thickness, in understanding the responses of different glacier types to climate change. We highlight the increased dependency of runoff from high Andean catchments on the diminishing resource of glacier ice during dry years.

Keywords: glacier mass balance, glacio-hydrological modelling, dry Andes of Chile, debris-covered glaciers, glacier runoff

1. Introduction

Seasonal snow and glacier melt in the semiarid Chilean Andes provide water to more than two thirds of Chile's population as well as maintaining key economic activities, ecosystems and ecosystem services (Favier et al., 2009). Central Chile is characterised by warm and dry summers, and humid cold winters, and ice melt provides a key contribution to runoff in dry periods and during late summer and autumn, in a water balance otherwise dominated by snowmelt (Ragettli and Pellicciotti, 2012; Ohlanders *et al.*, 2013; Ragettli *et al.*, 2013; Ayala *et al.*, 2016; Rodriguez *et al.*, 2016). While glaciers in the region have been receding and losing mass over the past few decades (Rivera *et al.*, 2002; Bown *et al.*, 2008; Mernild *et al.*, 2015; Malmros *et al.*, 2016; Ragettli *et al.*, 2016; Barcaza *et al.*, 2017), the runoff response to climate and glacier changes is still poorly understood. Recent trends of decreasing runoff from high elevation catchments (Casassa *et al.*, 2009; Mernild *et al.*, 2016; Ragettli *et al.*, 2016) suggest that the peak runoff, corresponding to the maximum contribution from a catchment (Pellicciotti *et al.*, 2010; Huss and Hock, 2018), was reached at some time in the past. Results obtained from advanced glacio-hydrological modelling at relatively high resolutions (Mernild *et al.*, 2016; Ragettli *et al.*, 2016) and trend analysis (Casassa *et al.*, 2009) are in agreement with global-scale models that also show declining trends in runoff from central Andean catchments (Bliss *et al.*, 2014; Huss and Hock, 2018). However, these analyses, have been based on either a few intensively studied glaciers (Ragettli *et al.*, 2016) or obtained from large scale studies with grid resolutions too coarse to capture differences caused by important local-scale processes (Mernild *et al.*, 2016, Huss and Hock, 2018). Multidecadal studies focusing on the processes generating glacier streamflow response to a changing climate are needed to bridge this scale gap.

Recent studies in the region have advanced our understanding of the spatial patterns of ablation and glacier mass balance (Ayala *et al.*, 2016, 2017; Bravo *et al.*, 2017), but they are

generally limited to a maximum of a few seasons of data and none has investigated decadal changes of mass balance and runoff. Time series analysis of observational records (Casassa *et al.*, 2009; Burger *et al.*, 2018) is a useful tool to establish general data trends, but is of limited use when observations are scarce in space and time, and cannot provide insights into which processes drive observed changes. Additionally, whilet satellite-based glacier inventories (Rivera *et al.*, 2002; Nicholson *et al.*, 2010; Rabatel *et al.*, 2011; Malmros *et al.*, 2016; Barcaza *et al.*, 2017) aided the establishment of baseline areal changes, they do not generally assess mass balance or volumes change, and cannot be used to explain the causes of observed changes. Therefore, there is a need for an integrated approach to understand the mid- and long-term changes in glaciers and glacier runoff in the high elevation catchments of the central Andes that combines both high resolution glacio-hydrological modelling and mass balance estimates from remote sensing (Pellicciotti et al., 2014), which are increasingly used to evaluate model simulations.

Determining glacier mass balance regimes and glacier hydrological contribution in the Andes is further complicated by the presence of debris-covered and rock glaciers, which account for approximately 3,200 km^2 of the 23,700 km^2 of inventoried ice (Barcaza *et al.*, 2017). While the contribution of these glaciers to high elevation streamflow is poorly understood (Ayala *et al.*, 2016), increasing evidence from other mountain regions shows a very distinct response of debris-covered glaciers to climate change compared to clean ice glaciers (Benn *et al.*, 2012; Rowan *et al.*, 2015). In one of the first glacio-hydrological modelling studies to explicitly include debris-covered glaciers, Ayala *et al.*, (2016) showed that the contribution of a debris-covered glacier to total runoff over two years was of a similar magnitude to that of two debris-free glaciers in the same catchment.

Here we take advantage of the rare opportunity afforded by a well instrumented catchment, the Rio del Yeso, to understand the interannual variability of glacier mass balance and glacier

contribution to runoff over a 16-year period at the start of the present century (2000-2015). Our main aims are to (1) reconstruct the glacier changes for the period 2000-2015 and (2) estimate the corresponding glacier contribution to runoff for the period. These aims are addressed through application of a physically-oriented and fully distributed glacio-hydrological model, in-situ data, and the first geodetic mass balance estimates for the region. We use this combination of modelling, field data and satellite observations to compare the hydrological contributions of a debris-covered glacier and two debris-free glaciers in the study catchment.

2 Study site and data

2.1 Study site

The Rio del Yeso catchment (33.55°S, 69.91°W, 3000-5230 m a.s.l, 62 km^2) is located ~70 km east of Santiago in the semiarid Andes of central Chile (Figure 1), and contains three principal glaciers: Bello, Yeso and Piramide. The former are small, debris-free valley-type glaciers (4.6 and 2.2 km^2, respectively), while the debris-covered Piramide Glacier covers a larger elevation gradient although has a total area similar to that of Bello Glacier (4.7 km^2). Piramide has a typical reverse ablation gradient and an estimated debris thickness ranging from 0.01 to 0.6 m (Ayala *et al.*, 2016, colour-scale in Figure 1a). Mixed snow-debris avalanches typically feed the highest elevations of the glacier from local headwalls.

2.2 Meteorological data

The model was forced with meteorological data (temperature and precipitation) from Yeso Embalse Automatic Weather station (AWS) from the Chilean Water Directorate (Dirección General de Aguas, DGA) meteorological network (Figure 1b). This AWS recorded daily maximum and minimum temperatures and daily precipitation for the entire simulation period (2000-2015). Additional temperature data from AWSs in the catchment were also used

(Table 1). Hourly and daily maximum and minimum temperature from the Laguna Negra AWS (2780 m a.s.l.) (Figure 1b) were used to identify the best disaggregation approach and evaluate the performance of the selected approach to derive hourly data from the temperature time series at Yeso Embalse AWS. Lapse rates used to extrapolate air temperature from Yeso Embalse AWS to the entire catchment were calculated using Yeso Embalse (2475 m a.s.l.), Yeso off-glacier (4300 m a.s.l.), Piramide off-glacier (3020 m a.s.l.), and Piramide on-glacier (3494 and 3655 m a.s.l.) AWSs (Figure 1c) between 2013 and 2015, using common data periods for each month (Table 2). Air temperature lapse rates were validated against hourly temperatures measured at AWSs installed on Bello and Yeso glaciers. Finally, daily cloud transmissivity coefficients were derived from reanalysis ERA-Interim data by considering constant values during the day.

2.3 Digital Elevation Models (DEMs)

Digital Elevation Models (DEMs) were used as both a basis for model runs (2000 SRTM at 30 m resolution), as well as to quantify glacier thinning through the 16-year simulation period. For the DEM differencing used to validate the model simulations we used the bistatic TanDEM-X and SRTM-C for the period 2000-2013, and two repeated airborne LiDAR surveys for 2012-2015. TerraSAR/X and TanDEM-X (TDX) correspond to an ongoing satellite constellation launched by the German Aerospace Center (DLR) and Airbus Defense and Space. TDX has a swath width of 30 km with a ground resolution of 0.4 arcsec. The Shuttle Radar Topography Mission (SRTM) was an interferometric synthetic aperture radar (InSAR) mission carried out simultaneously in the C- and X-band frequencies between 11 and 22 February 2000 between 56° S and 60° N (Farr *et al.*, 2007). We used the void-filled LPDAAC NASA version of the SRTM DEM at 1-arcsec resolution. The two airborne LiDAR

surveys carried out by the DGA have an estimated precision of ±0.30 m with an average of four points per square meter (ppm2) (DGA, 2012, 2015).

2.4 Terrestrial photographs

Daily photographs were taken by a time-lapse camera installed in front of Bello Glacier (Figure 1c) on 27 February 2014, covering an area of 0.84 km^2 (Ayala *et al.*, 2016), for which 48 valid photos are available between February to April 2014 and 114 between October 2014 to April 2015. The system included a Canon EOS Rebel T3 camera with a resolution of 12.2 MP and a focal length of 18 mm. The camera was programmed to take photos every day at 13 h (local time). Photos were georeferenced following Corripio (2004) and albedo was derived from the terrestrial photos as explained in Ayala et al. (2016).

3. Methods

3.1 TOPKAPI ETH model

We used the TOPKAPI-ETH model to simulate glacier mass balance, glacier changes and runoff generation in the Río del Yeso catchment. TOPKAPI-ETH is an extended version of the original rainfall-runoff model TOPKAPI (TOPographic Kinematic APproximation and Integration) (Liu and Todini, 2002, and Ciarapica and Todini, 2002) and it has been applied in glacierized catchments from a few tens to more than 30,000 km^2 in the semiarid Andes (Ragettli and Pellicciotti, 2012; Ragettli *et al.*, 2014a; Ayala *et al.*, 2016), the Swiss Alps (Finger *et al.*, 2011, 2012, Fatichi *et al.*, 2014, 2015) and the Himalaya (Ragettli *et al.*, 2013, 2014b, 2016).

TOPKAPI-ETH offers a compromise between a detailed representation of high-mountain hydrological processes and computational efficiency. The model incorporates physically-

based parameterizations of most relevant hydrological processes in high-mountain catchments, such as snow and ice melt (Pellicciotti *et al.*, 2005), ice melt under debris (Carenzo *et al.*, 2016), glacier area and elevation changes (Huss *et al.*, 2010), snow albedo decay (Brock *et al.*, 2000), gravitational redistribution of snow (Bernhardt and Schulz, 2010), and englacial storage and release of snow and ice meltwater (Hock and Noetzli, 1997).

In this study, we used the same TOPKAPI-ETH model setup as described in Ayala *et al.* (2016). Ayala et al. (2016) extensively calibrated and validated the model for the Rio del Yeso catchment using two years (2013-2015) of field data that included manual snow depth measurements, ablation stakes, meteorological data from four AWSs, albedo time series from radiation measurements at Bello and Yeso AWSs, distributed fields of daily albedo derived from optical photos, and streamflow measurements at the outlet of Bello and Yeso glaciers. To avoid error compensation and parameter ambiguity, the model was calibrated in a stepwise approach, in which each main parameter set was calibrated individually against specific field observations (see Figure 2 in Ayala et al., 2016). Here we perform an additional calibration step to account for the uncertainty in precipitation over the longer period of record of this study (see Section 3.5 below).

Using the calibrated model setup, we then simulate glacier mass balance, elevation and areal changes for the period 2000 to 2015. Glacier volume and geometry changes were simulated using the Δh-parametrization developed by Huss *et al.* (2010). The Δh-parametrization is an empirical method that quantifies ice thickness changes as a function of previously observed elevation changes, and was developed based on a large datasets of glaciers in the Swiss Alps (Huss *et al.*, 2010). Given the lack of repeated DEMs or ice volume observations for our region, we have used the set of parameters originally calibrated by Huss *et al.* (2010) for glaciers with an area smaller than 5 km^2. The model was run for 10 years in a spin up mode

to produce initial conditions of albedo and snow height and simulations started in 2000 with these initial conditions.

3.2 Extrapolation of meteorological variables

To drive the glacio-hydrological model, both air temperature and precipitation measurements are required at hourly resolution. While there was relatively good spatial coverage of AWSs in the study catchment in 2013-15, only a few stations were available over the complete study period (Table 1), and so data were extrapolated in both space and time. Hourly temperature time series were calculated from daily minimum and maximum values recorded at the Yeso Embalse AWS using the method suggested by Wilkerson *et al.* (1983), and adapted by Reicosky *et al.* (1989) (subroutine WCALC). The approach uses a sinusoidal function to interpolate between extreme values by dividing the day into three time periods: midnight to sunrise plus two hours; daylight hours; and sunset to midnight. It assumes that the minimum value occurs two hours after sunrise and the maximum halfway between sunrise and sunset time, obtained from the matlab subroutine Sunset, based on Montenbruck and Pfleger, (2000).

To evaluate the results of this approach in the study catchment, the method was tested at Laguna Negra AWS (LN, 2780 m a.s.l.; Figure 1b) using the data available for 2013-2015. This site was selected because daily minimum and maximum data as well as independently recorded hourly data were available, and the station was at a similar elevation to the Yeso Embalse AWS (Table 1). The evaluation resulted in a Nash-Sutcliffe model efficiency (NSE) criterion of 0.93.

The interpolated hourly temperature data were distributed from the Yeso Embalse (YE) AWS (Figure 1b) to the rest of the catchment using monthly means of hourly lapse rates, calculated from the available meteorological data in the catchment for each month and year with

concurrent data (Table 2). In order to represent the effect of the glacier boundary layer (Greuell and Böhm, 1998; Brock *et al.*, 2010), we use a parameter to decrease air temperature over glacier surfaces (Tmod) by subtracting 1°C for debris–free areas and a $Tmod_{debris}$ of 0.3°C to increase temperature for debris cover grid cells, calibrated for glacier-covered areas by Ayala *et al.* (2016). Figures 2 and 3 show the disaggregated and extrapolated temperatures at the Bello (Figure 2) and Yeso (Figure 3) AWSs. In general, calculated temperatures correspond well to measured values, especially during the daytime in the summer months; however the disaggregation and extrapolation method performs less well on glacier surfaces before sunrise when there snow was present, and during winter time when air temperatures were below 0° C.

Precipitation is not evenly distributed across the study catchment, and according to previous studies in the region, a logarithmic model can be used to represent precipitation spatial variability at high elevations (Vicuña *et al.*, 2010; Ragettli *et al.*, 2014a). Thus, we extrapolated the hourly precipitation measurements from Yeso Embalse AWS for the period 2000 to 2015 using a logarithmic model as follows (Ragettli *et al.*, 2014a):

$$P(z) = P(Yeso\ Embalse) \cdot (0.3866 \cdot \log(z) - 2.014) \qquad \text{Equation 1}$$

Where P(Yeso Embalse) is precipitation measured at Yeso Embalse, and P(z) the precipitation at the elevation "z". The values of the coefficients in Equation 1 were estimated from the logarithmic fit of the annual mean precipitation at 15 stations in the Maipo catchment for the period 2000-2015. Using a number of stations from the larger Maipo catchment ensures that the large-scale, synoptic variability of the precipitation pattern is reproduced. To represent local effects on precipitation and its accumulation over glaciers, we used a local scaling factor that modifies precipitation over each glacier (Huss *et al.* (2008); Magnusson *et al.* 2011; Farinotti *et al.*, 2012). This factor was calibrated to match the simulated long-term glacier elevation changes with those derived from the geodetic mass

balance to account for local processes governing snow accumulation on glaciers. Use of a local scaling factor for each glacier was supported by evidence from field observations of preferential deposition, scouring, and snow removal by wind, that cannot be captured by a regional precipitation gradient. The local factor was calibrated against the elevation change of the period 2000-2013 obtained from the DEM differencing. The estimated factors were 0.74 for Bello and Yeso, and 1.88 for Piramide. A similar approach has been used by Magnusson et al. (2011) and Farinotti *et al.*, (2012), and in light of the lack of local observations, it is a plausible way of preventing precipitation uncertainty from dominating the modelling exercise. Finally, precipitation was disaggregated to hourly values by distributing daily values homogeneously during the day.

3.3 Debris Thickness estimation

We used the debris thickness map derived by Ayala et al. (2016) for the debris-covered areas on the Piramide, Bello and Yeso glaciers (Figure 1). The map was derived by solving the distributed energy balance of the debris-covered areas at the moment of acquisition of a Landsat 8 thermal image of the area at 90-m spatial resolution. This method was originally presented by Foster *et al.*, (2012) as a physically-oriented alternative to empirical relationships between surface temperature and debris thickness (e.g. Mihalcea et al., 2008). Different versions of the method have been subsequently presented (e.g. Rounce and McKinney, 2014) but several uncertainties are still associated with this approach, such as the debris temperature profiles, heat storage rate and turbulent heat fluxes (Schauwecker *et al.*, 2015; Ayala *et al.*, 2016). Technical details regarding the development of the debris thickness map can be found in Appendix 1 in Ayala *et al.* (2016).

3.4 Geodetic elevation change

In recent years, the geodetic method has been widely used to obtain glacier changes over short- or long-term periods (e.g. Rankl and Braun, 2016; Bolch *et al.*, 2017). The method, based on the differencing of digital elevation models (DEMs) can provide glacier changes over several years for large remote areas.

We followed the TDX processing scheme in Malz *et al.* (2018) using the GAMMA software. We acquired co-registered single look complex images (CoSSC) in HH polarization provided by DLR. All the TanDEM-X scenes along one track were concatenated and the strips processed by differential interferometry (DInSAR) (e.g. Malz *et al.*, 2018). We used the SRTM-C DEM as a reference and subtracted it from the bistatic TanDEM-X interferogram. For this, the topographic phase was simulated from the SRTM-C DEM using the TanDEM-X orbit parameters. We unwrapped the interferograms using a Minimum Cost Flow algorithm. In order to remove the phase noise from the differential interferogram we applied a Goldstein filter, and areas with low coherence (coherence < 0.2) were masked out (Goldstein and Werner, 1998; Vijay et al.; 2016; Rankl and Braun, 2016). The unwrapped differential phase was converted into absolute differential heights. These differential heights were added back to the topographic heights from SRTM-C DEM to generate a TanDEM-X DEM. The resulting TanDEM-X DEMs were geocoded with the SRTM-C DEM to maintain planimetric consistency (e.g. Vijay *et al.*, 2016; Malz et al., 2018).

The post-processing comprises the mosaicking of all raw DEMs resulting from the InSAR strip processing. We used a stable ground mask derived from optical data (Landsat OLI 2013) and corrected vertical biases between the strips applying a polynomial fitting (Malz *et al.*, 2018). TanDEM-X DEMs were iteratively co-registered (vertically and laterally) to the SRTM-C DEM using the approach of Nuth and Kääb (2011).

Uncertainties in the geodetic elevation changes for the period 2000-2013 were estimated by calculating the Median Absolute Deviation (MAD) for the elevation differences on stable areas. Since the deviation is known to be slope-dependent (Gardelle *et al.*, 2012), the area of interest was divided in 5° slope-bins and the total MAD was calculated by weighting the area of each bin (e.g. Malz *et al.*, 2018). We discarded any significant bias associated to the radar signal penetration in snow and ice of SRTM-C and TanDEM-X, as previous studies have shown that summer DEM acquisitions in the Southern Hemisphere (during melting conditions) reveal negligible penetration (Jaber *et al.* 2013; Jaber *et al.* 2016; Falaschi *et al.*, 2017; Dussaillant *et al.*, 2018). As the LiDAR surveys included only a small portion of stable areas, we used the precision achieved by the LiDAR and GPS control points (±0.30 m) as an indication of the error for the period 2013-2015 (DGA, 2015). Finally, the uncertainties were estimated using the standard principles of error propagation.

3.5 Calibration and validation

A detailed scheme of the calibration and validation procedure is shown in Figure 4. The geodetic elevation difference for the 2000-2013 period was used to calibrate the precipitation correction factors over glacier surfaces (as described in Section 3.2), while the 2013-2015 dataset (obtained from LiDAR) was used to validate simulated ice elevation differences (Sections 2.3 and 3.4). Model simulations were also validated using albedo and snow covered area (SCA) obtained from processing terrestrial photos (Section 2.4), as well as albedo observations at AWSs in Bello and Yeso glaciers for the season 2014-2015 and SCA from MODIS. We compared the SCA derived from a daily MODIS MOD10A1 product (Hall *et al.*, 2002) to the catchment-wide snow cover area derived from the TOPKAPI-ETH on a daily timestep. The daily MODIS data were discarded if more than 10% of the total area was covered by cloud, and any remaining cloud covered cells were filtered using a linear interpolation of SCA quantity based upon a temporal search window of two days either side

of the cloud cover observation at the given cell. The MODIS grids were resampled to a 30 m grid and clipped to the same area as the model domain (see blue line in Figure 1c), and for each day, the catchment average SCA was extracted and compared to that of the TOPKAPI-ETH model simulations. The validation procedure of albedo and SCA using the terrestrial camera is detailed in Ayala et al. (2016) and not repeated here.

4. Results

4.1 Model validation results

The ground-based and satellite validations of the TOPKAPI-ETH model are given in Figures 5 and 6, respectively. The model captures the variability in albedo measured at Bello and Yeso AWSs and both the albedo and SCA derived from the terrestrial camera (Figure 5). Specifically, modelled albedo at Bello Glacier AWS follows the measured decay rates and albedo increase after spring storm events (Figure 5b), but it overestimates albedo at the Yeso Glacier AWS (Figure 5c), despite capturing the magnitude of the snow albedo decay at the start of 2014. The average albedo and SCA calculated from the camera photos (Figures 5d and e) are replicated over Bello Glacier with a slight tendency towards over-estimation in the spring months (October-November). In summer (January 2015), the albedo simulations perform particularly well (RMSE = 0.19).

At the catchment scale, TOPKAPI-ETH simulates the timing of snow cover disappearance of the daily MODIS SCA product (Figure 6). In the period 2001 to 2009, the appearance and disappearance of snow is well reproduced, with a RMSE of ~11-15% for individual years. After 2010, the model performance declines, and the timing of the snow cover disappearance in the spring and summer is not well reproduced (RMSE >20%). The total summer SCA minimums, however, are in line with the MODIS results, which suggests that in general the model can capture the seasonal variability of snow cover.

4.2 Glacier elevation changes

Results from the geodetic elevation change show generally positive or stable values for the 13 years from 2000 to 2013 (Figures 7a-b), and then a generally negative mass balance in the period 2013-2015 (Figures 7c-d). The change in the second period is noteworthy, with an ice thinning rate of -1.15 ± 0.15 m yr^{-1} (-2.31 ± 0.30 m) for Bello Glacier, in contrast with a mean rate of -0.01 ± 0.09 m yr^{-1} (-0.15 ± 1.23 m) for the period 2000-2013 (Table 3). Yeso Glacier has similar thinning rates of -0.03 ± 0.09 m yr^{-1} (-0.43 ± 1.23 m) for the period 2000-2013, and -1.08 ± 0.15 m yr^{-1} (-2.17 ± 0.30 m) for the subsequent period.

For 2013-2015, the highest mass losses on Piramide Glacier are observed in the upper section (Figure 7d), where debris is thin (Figure 1a). Comparatively, there is a smaller loss on the lower tongue, and the lowest elevation differences are observed in the central section of the glacier (Figure 7d). Areas of thick debris interspersed with ice cliffs are characterised by heterogeneous surface differences for both periods (Figures 7b and 7d). For the latter period (2013-2015), the reduction of snow accumulation for the upper Piramide Glacier resulted in greater surface lowering (Figure 7d) where debris is thin and snow is normally supplied by high avalanche loads.

TOPKAPI-ETH simulations show an initial positive glacier elevation change followed by a neutral or slightly negative change for the two debris-free glaciers (Bello and Yeso) for the period 2000-2013, while estimates for the debris-covered Piramide glacier indicate an initial ice thickness increase followed by a decline in 2009 until reaching cumulative negative values of approximately -3.4 m in 2015 (Figure 8). Bello and Yeso lag behind Piramide, showing strong thickness decreases is the final two years and a lower cumulative decrease by 2015 than at Piramide (Figure 8).

There is considerable spatial variability in mass balance, with distinct patterns for each glacier (Figures 9a-c). The surface height changes of Bello and Yeso become more positive

with increasing elevation, and are particularly negative for thin debris areas on the tongue of Yeso Glacier (between 3900-4100 m a.s.l.). The simulated profile of surface height change on Piramide Glacier peaks in the mid-glacier area for the period 2000-2013, with a slight increase with elevation for both periods between 3200 and 3700 m a.s.l. (corresponding to areas of thick debris), and then positive mass balance for the period 2000-2013 between 3800 and 4200 m a.s.l., in correspondence with the areas of highest avalanche mass mobilization (results not shown). The mass balance is also negative between 4200 m a.s.l. and the upper reaches of the glacier at 4600 m a.s.l., which correspond to areas of thin debris cover (Figure 1a), where an elevation gradient is re-established (Figure 9c).

The geodetic elevation changes show a similar pattern as simulations over Yeso and Bello for the final three years of the study period (Figures 9a-b). However, geodetic values were more negative than the 2000-2013 simulations between 4200 and 4800 m a.s.l. (Figures 9a-b).

The differences between the debris-free and debris-covered glaciers are also evident in the spatial distribution of the geodetic mass balance, with a profile that is quite smooth for Bello (and slightly less so for Yeso) while the spatial variability at Piramide is very high, a feature also well captured by the model. According to the geodetic mass balance between 2000 and 2013, simulations in Bello and Yeso overestimate melt below ~4300 m a.s.l., and overestimate accumulation above that elevation, while at Piramide the geodetic mass balance pattern for that period is similar to the simulations, with a small melt overestimation between 3500 and 3800 m a.s.l.

4.3 Runoff and runoff components

Total runoff and the annual contribution to runoff from snowmelt, icemelt and precipitation are shown in Figure 10. A clear overall decline in runoff can be observed, which is marked for the period after 2009. The main runoff contribution comes from snowmelt, accounting for 66 to 93% of total runoff per year. Icemelt contribution fluctuates between 3.5 and 32%, and

is highest in dry years with low total runoff (such as 2014-2015, which have the highest proportional contribution from icemelt). The liquid precipitation contribution is consistently small and does not exceed 6% in any given year. While annually snowmelt represents the main water input to the system, in summer (January and February) icemelt becomes increasingly dominant, contributing equally with snowmelt by March (Figure 11). The contribution of icemelt to total runoff from each of the three glaciers is distinct (Figure 12). Bello and Yeso have the smallest average icemelt runoff with 5.4 and $5.7 \cdot 10^{-5}$ m h^{-1}, respectively, while the highest icemelt contribution is from Piramide, with $8.3 \cdot 10^{-5}$ m h^{-1}. It should be noted that Bello Glacier displays larger inter-annual variations in streamflow contributions from icemelt than Piramide. Snowmelt contribution to total runoff from Bello and Yeso are 4.6 and $4.3 \cdot 10^{-5}$ m h^{-1} respectively, and Piramide has the highest snowmelt contribution of $1.59 \cdot 10^{-4}$ m h^{-1}, being the glacier with more snowmelt variability. Since 2011, snowmelt contribution from all three glaciers has reduced compared to the previous years (orange and red lines on the right hand panels in Figure 12). The seasonality is also distinct from 2013 onwards, with snowmelt and icemelt both occurring earlier at Piramide (Figure 12e and f) than on the other two glaciers (Figure 12a-d).

5. **Discussion**

5.1 Mass balance and runoff contribution

Geodetic mass balance estimates show a very distinct behaviour in the two analysed periods (2000-2013 and 2013-2015). While an almost neutral elevation change was obtained for the first period (-0.01 to -0.14 m yr^{-1}), a high ice thinning rate is evident for the second period (-0.75 to -1.16 m yr^{-1}). An important asset of model simulations is that they allow the identification of different mass balance trends between the acquisition times of the DEMs used in the geodetic change detection. In this case, results from TOPKAPI-ETH suggest that the neutral mass balance of the period 2000-2013 is a result of a moderate positive trend in

2000-2009 and a strong negative trend in 2010-2013, which continued in 2013-2015. These results agree with the mass balance measurements on Echaurren Norte Glacier, the only long-term glacier mass balance monitoring program in the Andes of central Chile, which shows similar patterns from the year 2000 (Masiokas *et al.*, 2016), having four years of positive mass balance between 2000-2009 and no positive mass balance years since then (Masiokas et al., 2016, WGMS, 2017). The strong negative trend in glacier mass balance observed from 2010 is clearly related to the severe drought observed in the Chilean central regions during recent years (Garreaud *et al.*, 2017), termed the "Mega-drought" (Boisier *et al.*, 2016) which has been characterized by historically low precipitation levels, shallow seasonal snowpacks (Cornwell *et al.*, 2016; Cortés and Margulis, 2017) and high temperatures (Garreaud *et al.*, 2017), especially in spring and autumn (Burger *et al.*, 2018).

There is a good agreement between the simulated and geodetic mass balance at Piramide Glacier (Figure 8). The model does not fully reproduce the values from the geodetic mass balance at Bello and Yeso glaciers in 2015, though they are within the range of uncertainties of the geodetic measurements. Simulations do show a decreasing trend starting in 2010, but the geodetic mass loss in the period 2010-2015 is larger than that from the model. Despite these differences, a more detailed analysis of the patterns of glacier surface change shows that the model is able to reproduce some of the elevation-dependent differences evident in the geodetic elevation changes (Figure 9). Importantly, the model is able to resolve much of the spatial variability of glacier surface change in relation to the differences in debris thicknesses, as well as those related to the avalanches that feed the debris-covered Piramide glacier.

The glaciers analysed in this study provide an excellent example of the different processes that affect the long-term evolution of debris-free and debris-covered glaciers within one catchment. While the mass balance of Bello and Yeso is more strongly controlled by temperature gradients affecting the precipitation phase and ablation components of the model

(Ayala et al., 2016) and snow removal on the mid glacier (evidence from unpublished data on Bello), the mass balance of Piramide Glacier is controlled principally by debris thickness and snow accumulation from avalanches (Figure 9). A sensitivity analysis revealed that ignoring the contribution of avalanching in the model simulations produces a total cumulative elevation change more than three times more negative for Piramide compared to our reference model (Figure 13). Ignoring this process has a greater impact on the total absolute glacier elevation change than artificially providing 10 centimetres more surface debris for the glacier (red triangles in Figure 13). The strong control that debris thickness exerts over the glacier mass balance has been extensively demonstrated in the literature (e.g. Ragettli *et al.*, 2016; Vincent *et al.*, 2016) and is shown by the results from our study to be important for long term modelling of debris-covered glaciers mass balance.

The removal of snow from the central sections of Bello Glacier would contradict a hypothesis that glacier areas act as net sinks of snow during the accumulation season (Dadic. *et al.*, 2010; Gascoin *et al.*, 2013). However, the mass losses that seem to occur on Bello and Yeso glaciers might be compensated by the contribution of avalanches from the surrounding upper slopes, which is still shown to be an important process for these glaciers (Figure 13). Evidence of negative surface changes in the central sections of Bello (Figure 7a) reveals a potential local process of wind effects on snow which agrees with field observations, though modelling snow redistribution on high elevation glaciers remains an important area for future studies, even if outside of the scope of this paper.

Runoff generation from debris-free and debris-covered glaciers also exhibit a distinct behaviour. Particularly interesting is the different interannual spread in the runoff generated by icemelt from Bello and Piramide glaciers (Figure 12). Icemelt from Bello Glacier shows a large interannual variability, which most likely indicates a sensitivity to climatic variability of precipitation and temperature. In turn, icemelt from Piramide Glacier is largely insulated

from climatic changes due to its supraglacial debris. Interestingly, the opposite pattern is evident for snowmelt, i.e. large interannual variability on Piramide Glacier in comparison with Bello Glacier (Figure 12f). In this case, the predominant low elevation of Piramide Glacier makes the snowpack sensitive to air temperature and the proportional amounts of solid winter precipitation. Further still, the mass loss characteristics of a debris-covered glacier such Piramide Glacier is strongly governed by the presence of ice cliffs (Steiner *et al.*, 2015; Buri *et al.*, 2016) which are currently not considered in TOPKAPI-ETH. Future modelling studies of debris-covered glaciers may therefore benefit from physically-based or parameterised representations of these processes.

As demonstrated by previous studies for individual years, snowmelt is the largest contributor to runoff in Andean catchments of central Chile with an outlet point around 3000 m a.s.l. (Ragettli and Pellicciotti, 2012; Ohlanders *et al.*, 2013). In this study, we showed that this result holds for a long time period, although with important interannual variability (Figure 10). Particularly important is the evidence that icemelt contribution becomes more relevant during drought periods. We observed an increase in the relative contribution to runoff of ice melt from 11.6% in the period 2000-2009 to 20.5% in the period 2010-2015. Quantifying the shift in relative streamflow contributions for a drier climate is highly relevant to the socio-economy of central Chile, and our study provides a new insight into the longer term evolution of these contributions, and most significantly a shift to increasing dependency on the declining resource of glacier ice.

5.2 Sources of uncertainty

As suggested by Ayala et al. (2016), the spatial distribution of forcing variables and the debris thickness are relevant controls on the glacier mass balance in this catchment. Particularly challenging is the modelling of snow accumulation on debris-free glaciers and wind-exposed locations. As our simulations show, the cumulative elevation change of Bello

and Yeso glaciers was consistently overestimated when using regional precipitation gradients that provide a good representation of annual water balances in the region. More precise regional estimates of precipitation and the simulation or parameterization of snow transport would likely improve the simulation of glacier mass balance. On the other hand, more accurate estimates of the current debris thickness distribution and its time evolution will become necessary for future studies on long-term glacier mass balances (Rowan *et al.*, 2015). However, changes in debris thickness over a period of 16 years are likely minor or restricted to specific areas.

6. Conclusion

In this paper, we have used a combination of distributed glacio-hydrological modelling, new estimates of geodetic mass balance for the region and a large amount of field data over two seasons to investigate the mass balance and runoff contribution of the glaciers of the Rio del Yeso catchment. Our main conclusions are:

- The glaciers of the study catchment experienced a period of positive or near-neutral surface elevation change for much of the early 21st Century (until 2008 and 2012 for Piramide and the debris free glaciers, respectively), suggesting that they have been in equilibrium with climate over that period. The period of neutral or positive elevation change was followed by a negative trend coinciding with a severe 'mega-drought' that has affected central Chile since 2010. The positive elevation changes observed in the first 9 years of our period are consistent with years of positive mass balance in Echaurren glacier between 2000 and 2009. It is only the scarce precipitation associated with the mega-drought that re-established the conditions for strong ablation and thus important mass losses.
- The spatial distribution of the mass balance over the debris-covered glacier is distinct to that of the debris-free glaciers, and its elevation profile is related most strongly to

the debris thickness variability and avalanches contribution. There is also a contrast in behaviour in terms of runoff contribution between the debris-covered and debris-free glaciers. The interannual variability of snowmelt contributions from Piramide Glacier is much larger and more sensitive to the 0°C isotherm than the debris-free Bello and Yeso glaciers. By contrast, there is a less variable interannual sub-debris icemelt on Piramide Glacier that is decoupled from high frequency climate variability.

- We witness a clear decrease in runoff over the period of study, with very low runoff during the years of the mega-drought, but a decline which is evident from the start of the study period in 2000. Our period of record is too short to confirm a general long-term trend, such as those that have been modelled or suggested by other studies in the region. Dry years show an increased dependency of runoff on the declining resource of glacier ice.

Given this result and those of the global studies, there is a clear need to extend model simulations and reconstruction of geodetic elevation changes for debris-free and debris-covered glaciers to longer time periods, in order to establish whether the peak water has been reached already and what the contribution of distinct types of glaciers is.

Acknowledgments

Meteorological data were provided by the Chilean Water Authority (Dirección General de Aguas, DGA) and the National Meterological Service (Dirección Meteorológica de Chile, DMC). Derivation of the geodetic mass balance was kindly supported by DLR (German Aerospace Center) with TanDEM-X data under DLR AO XTI_GLAC0264. Landsat TM and SRTM-C were provided by USGS and LiDAR data were kindly provided by DGA. F. Burger and D. Farias acknowledge the support from National Committee Sciences and Technology of Chile (CONICYT) through the Chilean scholarship program Becas Chile. Additionally, we

would like to thank members from CEAZA and the Universidad de Chile who supported the field campaigns that generated datasets used in this study. Data were collected within the project 'Modelling the mass balance and water discharges from glaciers of North-Central Chile' (S.I.T. N 382), funded by the Chilean Water Authority (Dirección General de Aguas, DGA), which is kindly acknowledged. We are very thankful to two anonymous reviewers that provided important comments to improve this manuscript.

References

Ayala A, Pellicciotti F, Burlando P. 2017. Melt and surface sublimation across a glacier in a dry environment: distributed energy-balance modelling of Juncal Norte Glacier, Chile. *Journal of Glaciology* **63**: 1–20 DOI: 10.1017/jog.2017.46

Ayala A, Pellicciotti F, MacDonell S, McPhee J, Vivero S, Campos C, Egli P. 2016. Modelling the hydrological response of debris-free and debris- covered glaciers to present climatic conditions in the semiarid Andes of central Chile. *Hydrological Processes* **30**: 4036–4058 DOI: 10.1002/hyp.10971

Barcaza G, Nussbaumer SU, Tapia G, Valdés J, García JL, Videla Y, Albornoz A, Arias V. 2017. Glacier inventory and recent glacier variations in the Andes of Chile, South America. *Annals of Glaciology*: 1–15 DOI: 10.1017/aog.2017.28

Benn D, Thompson S, Gulley J, Mertes J, Luckman A, Nicholson L. 2017. Structure and evolution of the drainage system of a Himalayan debris-covered glacier, and its relationship with patterns of mass loss. *Cryosphere* **11** (5): 2247–2264 DOI: 10.5194/tc-11-2247-2017

Benn DI, Bolch T, Hands K, Gulley J, Luckman A, Nicholson LI, Quincey D, Thompson S,

Toumi R, Wiseman S. 2012. Response of debris-covered glaciers in the Mount Everest region to recent warming, and implications for outburst flood hazards. *Earth-Science Reviews* **114** (1–2): 156–174 DOI: 10.1016/j.earscirev.2012.03.008

Bernhardt M, Schulz K. 2010. SnowSlide: A simple routine for calculating gravitational snow transport. *Geophysical Research Letters* **37** (11): 1–6 DOI: 10.1029/2010GL043086

Bliss A, Hock R, Radić V. 2014. Global response of glacier runoff to twenty-first century climate change. *Journal of Geophysical Research* **119**: 1–14 DOI: 10.1002/2013JF002931.Received

Boisier JP, Rondanelli R, Garreaud RD, Muñoz F. 2016. Anthropogenic and natural contributions to the Southeast Pacific precipitation decline and recent mega-drought in central Chile. *Geophysical Research Letters* **43** (1): 413–421 DOI: 10.1002/2015GL067265

Bolch T, Pieczonka T, Mukherjee K, Shea J. 2017. Brief communication: Glaciers in the Hunza catchment (Karakoram) have been nearly in balance since the 1970s, *The Cryosphere* **11**, 531-539, https://doi.org/10.5194/tc-11-531-2017.

Bown F, Rivera A, Acuña C. 2008. Recent glacier variations at the Aconcagua basin, central Chilean Andes. *Annals of Glaciology* **48** (1): 43–48 DOI: 10.3189/172756408784700572

Bravo C, Loriaux T, Rivera A, Brock BW. 2017. Assessing glacier melt contribution to streamflow at Universidad Glacier, central Andes of Chile. *Hydrology and Earth System Sciences* **21** (7): 3249–3266 DOI: 10.5194/hess-21-3249-2017

Brock B, Mihalcea C, Kirkbride MP, Diolaiuti G, Cutler MEJ, Smiraglia C. 2010.

Meteorology and surface energy fluxes in the 2005–2007 ablation seasons at the Miage debris-covered glacier, Mont Blanc Massif, Italian Alps. *Journal of Geophysical Research* **115** (D9): D09106 DOI: 10.1029/2009JD013224

Brock BW, Willis IC, Sharp MJ. 2000. Measurement and parameterisation of albedo variations at Haut Glacier d ' Arolla , Switzerland. *Journal of Glaciology* **46** (155): 675–688 DOI: 10.3189/172756506781828746

Burger F, Brock B, Montecinos A. 2018. Seasonal and elevational contrasts in temperature trends in Central Chile between 1979 and 2015. *Global and Planetary Change* **162**: 136–147 DOI: 10.1016/j.gloplacha.2018.01.005

Buri P, Pellicciotti F, Steiner JF, Miles ES, Immerzeel WW. 2016. A grid-based model of backwasting of supraglacial ice cliffs on debris-covered glaciers. *Annals of Glaciology* **57** (71): 199–211 DOI: 10.3189/2016AoG71A059

Carenzo M, Pellicciotti F, Mabillard J, Reid T, Brock BW. 2016. An enhanced debris temperature index model accounting for thickness effect. *Advances in Water Resources* **94**: 457–469 DOI: 10.1016/j.advwatres.2016.05.001

Casassa G, López P, Pouyaud B, Escobar F. 2009. Detection of changes in glacial run-off in alpine basins: examples from North America , the Alps , central Asia and the Andes. *Hydrological Processes* **23**: 31–41 DOI: 10.1002/hyp

Ciarapica L, Todini E. 2002. TOPKAPI: A model for the representation of the rainfall-runoff process at different scales. *Hydrological Processes* **16** (2): 207–229 DOI: 10.1002/hyp.342

Cogley JG, Hock R, Rasmussen LA, Arendt AA, Bauder A, Braithwaite RJ, Jansson P, Kaser G, Möller M, Nicholson L, et al. 2011. Glossary of Glacier Mass Balance and Related

Terms. Paris.

Cornwell E, Molotch NP, McPhee J. 2016. Spatio-temporal variability of snow water equivalent in the extra-tropical Andes Cordillera from distributed energy balance modeling and remotely sensed snow cover. *Hydrology and Earth System Sciences* **20** (1): 411–430 DOI: 10.5194/hess-20-411-2016

Corripio JG. 2004 Snow surface albedo estimation using terrestrial photography. *International Journal of Remote Sensing* **25**(24): 5705-5729 DOI: 10.1080/01431160410001709002

Cortés G, Margulis S. 2017. Impacts of El Niño and La Niña on interannual snow accumulation in the Andes: Results from a high-resolution 31 year reanalysis. *Geophysical Research Letters* **44** (13): 6859–6867 DOI: 10.1002/2017GL073826

Dadic R., Mott R, Lehning M, Burlando P. 2010. Wind influence on snow depth distribution and accumulation over glaciers. *Journal of Geophysical Research* **115** (F1) DOI: 10.1029/2009JF001261

DGA. 2012. Levantamiento láser aerotransportado y topografía superficial de glaciares en Chile Central. Santiago.

DGA. 2015. Modelo Digital de Elevación de centros montañosos y glaciares de las zonas glaciológicas Norte y Centro mediante LiDAR Aerotranpsortado. Santiago.

Dussaillant I, Berthier E, Brun F. 2018. Geodetic Mass Balance of the Northern Patagonian Icefield from 2000 to 2012 Using Two Independent Methods. *Frontiers in Earth Science* **6** (February): 1–13 DOI: 10.3389/feart.2018.00008

Falaschi D, Bolch T, Rastner P, Lenzano MG, Lenzano L, Lo Vecchio A, Moragues S. 2017. Mass changes of alpine glaciers at the eastern margin of the Northern and Southern Patagonian Icefields between 2000 and 2012. *Journal of Glaciology* **63** (238): 258–272 DOI: 10.1017/jog.2016.136

Farinotti, D., Usselmann, S., Huss, M., Bauder, A., Funk, M., 2012. Runoff evolution in the Swiss Alps: Projections for selected high-alpine catchments based on ENSEMBLES scenarios. *Hydrological Processes* **26**, 1909–1924.

Farr T, Rosen P, Caro E, Crippen R, Duren R, Hensley S, Kobrick M, Paller M, Rodriguez E, Roth L, et al. 2007. The shuttle radar topography mission. *Reviews of Geophysics* **45** (2005): 1–33 DOI: 10.1029/2005RG000183.1.INTRODUCTION

Fatichi S, Rimkus S, Burlando P, Bordoy R. 2014. Does internal climate variability overwhelm climate change signals in streamflow? The upper Po and Rhone basin case studies. *Science of the Total Environment* **493**: 1171–1182 DOI: 10.1016/j.scitotenv.2013.12.014

Fatichi S, Rimkus S, Burlando P, Bordoy R, Molnar P. 2015. High-resolution distributed evaluation of climate and anthropogenic changes on the hydrology of an Alpine catchment. *Journal of Hydrology* **525**: 362–382 DOI: 10.1016/j.jhydrol.2015.03.036

Favier V, Falvey M, Rabatel A, Praderio E, López D. 2009. Interpreting discrepancies between discharge and precipitation in high-altitude area of chile's norte chico region (26-32°S). *Water Resources Research* **45** (2): 1–20 DOI: 10.1029/2008WR006802

Finger D, Heinrich G, Gobiet A, Bauder A. 2012. Projections of future water resources and their uncertainty in a glacierized catchment in the Swiss Alps and the subsequent effects on hydropower production during the 21st century. *Water Resources Research* **48** (2):

1–20 DOI: 10.1029/2011WR010733

Finger D, Pellicciotti F, Konz M, Rimkus S, Burlando P. 2011. The value of glacier mass balance, satellite snow cover images, and hourly discharge for improving the performance of a physically based distributed hydrological model. *Water Resour. Res.* **47** (7): 1–14 DOI: 10.1029/2010WR009824

Foster LA, Brock BW, Cutler MEJ, Diotri F. 2012. A physically based method for estimating supraglacial debris thickness from thermal band remote-sensing data. *Journal of Glaciology* **58** (210): 677–691 DOI: 10.3189/2012JoG11J194

G. Wilkerson G, W. Jones J, J. Boote K, T. Ingram K, W. Mishoe J. 1983. Modeling Soybean Growth for Crop Management. *Transactions of the ASAE* **26** (1): 63 DOI: https://doi.org/10.13031/2013.33877

Gardelle J, Berthier E, Arnaud Y. 2012. Impact of resolution and radar penetration on glacier elevation changes computed from DEM differencing. *Journal of Glaciology* **58** (208): 419–422 DOI: 10.3189/2012JoG11J175

Garreaud R, Alvarez-Garreton C, Barichivich J, Boisier JP, Christie D, Galleguillos M, LeQuesne C, McPhee J, Zambrano-Bigiarini M. 2017. The 2010-2015 mega drought in Central Chile: Impacts on regional hydroclimate and vegetation. *Hydrology and Earth System Sciences Discussions* (April): 1–37 DOI: 10.5194/hess-2017-191

Gascoin S, Lhermitte S, Kinnard C, Bortels K, Liston GE. 2013. Wind effects on snow cover in Pascua-Lama, Dry Andes of Chile. *Advances in Water Resources* **55**: 25–39 DOI: 10.1016/j.advwatres.2012.11.013

Goldstein RM, Werner CL. 1998. Radar interferogram filtering for geophysical applications. Geophys. Res. Lett., 25(21), 4035– 4038 (doi: 10.1029/1998GL900033).

Greuell W, Böhm R. 1998. 2 M Temperatures Along Melting Mid-Latitude Glaciers, and Implications for the Sensitivity of the Mass Balance To Variations in Temperature. *Journal of Glaciology* **44** (146): 9–20

Hall DK, Riggs GA, Salomonson V V, Digirolamo NE, Bayr KJ. 2002. MODIS snow-cover products. *Remote Sensing of Environment* **83**: 181–194 DOI: 10.1016/S0034-4257(02)00095-0

Hock R, Noetzli C. 1997. Areal melt and discharge modelling of Storglaciären. *Annals of Glaciology* **24**: 211–216

Huss M, Hock R. 2018. Global-scale hydrological response to future glacier mass loss. *Nature Climate Change* DOI: 10.1038/s41558-017-0049-x

Huss M, Farinotti D, Bauder A, Funk M. 2008. Modelling runoff from highly glacierized alpine drainage basins in a changing climate. *Hydrological Processes* **22** (November 2008): 3888–3902 DOI: 10.1002/hyp.7055

Huss M, Jouvet G, Farinotti D, Bauder A. 2010. Future high-mountain hydrology: A new parameterization of glacier retreat. *Hydrology and Earth System Sciences* **14** (5): 815–829 DOI: 10.5194/hess-14-815-2010

Jaber, W.A., Floricioiu, D., Rott, H., Eineder, M., 2013. Surface elevation changes of glaciers derived from SRTM and TanDEM-X DEM differences. In: 2013 IEEE International Geoscience and Remote Sensing Symposium - IGARSS. pp. 1893–1896.

Jaber, W.A., Floricioiu, D., Rott, 2016. Geodetic mass balance of the Patagonian Icefields derived from SRTM and TanDEM-X data. In: 2016 IEEE International Geoscience and Remote Sensing Symposium - IGARSS. Beijing, 2016, pp. 342-345. doi: 10.1109/IGARSS.2016.7729082

Kääb A, Berthier E, Nuth C, Gardelle J, Arnaud Y, Kaab A, Berthier E, Nuth C, Gardelle J, Arnaud Y. 2012. Contrasting patterns of early twenty-first-century glacier mass change in the Himalayas. *Nature* **488** (7412): 495–498 DOI: 10.1038/nature11324

Liu Z, Todini E. 2002. Towards a comprehensive physically-based rainfall-runoff model. *Hydrology and Earth System Sciences* **6** (5): 859–881 DOI: 10.5194/hess-6-859-2002

Magnusson J, Farinotti D, Jonas T, Bavay M. 2011. Quantitative evaluation of different hydrological modelling approaches in a partly glacierized Swiss watershed. *Hydrological Processes* **25** (13): 2071–2084 DOI: 10.1002/hyp.7958

Malmros JK, Mernild SH, Wilson R, Yde JC, Fensholt R. 2016. Glacier area changes in the central Chilean and Argentinean Andes 1955 – 2013. *Journal of Glaciology* **62** (232): 391–401 DOI: 10.1017/jog.2016.43

Malz P, Meier E, Cassasa G, Jaña R, Svarca P, Braun MH. 2018. Elevation and mass changes of the Southern Patagonia Icefield derived from TanDEM-X and SRTM data. *Remote Sensing* **10** (2)

Masiokas MH, Christie DA, Le Quesne C, Pitte P, Ruiz L, Villalba R, Luckman BH, Berthier E, Nussbaumer SU, González-Reyes A, et al. 2016. Reconstructing glacier mass balances in the Central Andes of Chile and Argentina using local and regional hydro-climatic data. *The Cryosphere* **10**: 927–940 DOI: 10.5194/tc-10-927-2016

Mernild SH, Beckerman AP, Yde JC, Hanna E, Malmros JK, Wilson R, Zemp M. 2015. Mass loss and imbalance of glaciers along the Andes Cordillera to the sub-Antarctic islands. *Global and Planetary Change* **133**: 109–119 DOI: 10.1016/j.gloplacha.2015.08.009

Mernild SH, Liston GE, Hiemstra CA, Yde JC, McPhee J, Malmros JK. 2016. The Andes

Cordillera. Part II: Rio Olivares Basin snow conditions (1979-2014), central Chile. *International Journal of Climatology* **37** (4): 1699–1715 DOI: 10.1002/joc.4828

Mihalcea C, Mayer C, Diolaiuti G, D'Agata C, Smiraglia C, Lambrecht A, Vuillermoz E, Tartari G. 2008. Spatial distribution of debris thickness and melting from remote-sensing and meteorological data, at debris-covered Baltoro glacier, Karakoram, Pakistan. *Annals of Glaciology* **48** (July 2004): 49–57 DOI: 10.3189/172756408784700680

Miles ES, Steiner J, Willis I, Buri P, Immerzeel WW, Chesnokova A, Pellicciotti F. 2017. Pond Dynamics and Supraglacial-Englacial Connectivity on Debris-Covered Lirung Glacier, Nepal. *Frontiers in Earth Science* **5** (September): 1–19 DOI: 10.3389/feart.2017.00069

Montenbruck, O., Pfleger, T., 2000. Special Perturbations. In: Astronomy on the Personal Computer. Springer, pp. 83–106.

Nicholson L, Marín J, Lopez D, Rabatel A, Bown F, Rivera A. 2010. Glacier inventory of the upper Huasco valley, Norte Chico, Chile: glacier characteristics, glacier change and comparison with central Chile. *Annals of Glaciology* **50** (53): 111–118 DOI: 10.3189/172756410790595787

Nuth C, Kääb A. 2011. Co-registration and bias corrections of satellite elevation data sets for quantifying glacier thickness change. *Cryosphere* **5** (1): 271–290 DOI: 10.5194/tc-5-271-2011

Ohlanders N, Rodriguez M, McPhee J. 2013. Stable water isotope variation in a Central Andean watershed dominated by glacier and snowmelt. *Hydrology and Earth System Sciences* **17** (3): 1035–1050 DOI: 10.5194/hess-17-1035-2013

Pellicciotti F, Bauder A, Parola M. 2010. Effect of glaciers on streamflow trends in the Swiss Alps. *Water Resources Research* **46** (10): 1–16 DOI: 10.1029/2009WR009039

Pellicciotti F, Brock B, Strasser U, Burlando P, Funk M, Corripio J. 2005. An enhanced temperature-index glacier melt model including the shortwave radiation balance: development and testing for Haut Glacier d'Arolla, Switzerland. *Journal of Glaciology* **51** (175): 573–587 DOI: 10.3189/172756505781829124

Pritchard H. 2017. Asia's glaciers are a regionally important buffer against drought. *Nature* **545** (7653): 169–174 DOI: 10.1038/nature22062

Rabatel A, Castebrunet H, Favier V, Nicholson L, Kinnard C. 2011. Glacier changes in the Pascua-Lama region, Chilean Andes (29° S): Recent mass balance and 50 yr surface area variations. *Cryosphere* **5** (4): 1029–1041 DOI: 10.5194/tc-5-1029-2011

Ragettli S, Pellicciotti F. 2012. Calibration of a physically based, spatially distributed hydrological model in a glacierized basin: On the use of knowledge from glaciometeorological processes to constrain model parameters. *Water Resources Research* **48** (3) DOI: 10.1029/2011WR010559

Ragettli S, Cortes G, Mcphee J, Pellicciotti F. 2014a. An evaluation of approaches for modelling hydrological processes in high-elevation, glacierized Andean watersheds. *Hydrological Processes* **28** (23): 5674–5695 DOI: 10.1002/hyp.10055

Ragettli S, Immerzeel WW, Pellicciotti F. 2016. Contrasting climate change impact on river flows from high-altitude catchments in the Himalayan and Andes Mountains. *Proceedings of the National Academy of Sciences of the United States of America* **113** (33): 9222–7 DOI: 10.1073/pnas.1606526113

Ragettli S, Pellicciotti F, Bordoy R, Immerzeel WW. 2013. Sources of uncertainty in

modeling the glaciohydrological response of a Karakoram watershed to climate change. *Water Resources Research* **49** (9): 6048–6066 DOI: 10.1002/wrcr.20450

Ragettli S, Pellicciotti F, Immerzeel WW, Miles ES, Petersen L, Heynen M, Shea JM, Stumm D, Joshi S, Shrestha AB. 2014b. Unraveling the hydrology of a Himalayan catchment through integration of high resolution in situ data and remote sensing with an advanced simulation model. *Advances in Water Resources* **78** (September): 94–111 DOI: 10.1016/j.advwatres.2015.01.013

Rankl M, Braun M. 2016. Glacier elevation and mass changes over the central Karakoram region estimated from TanDEM-X and SRTM/X-SAR digital elevation models. *Annals of Glaciology* **57** (71): 273–281 DOI: 10.3189/2016AoG71A024

Reicosky DC, Winkelman LJ, Baker JM, Baker DG. 1989. Accuracy of hourly air temperatures calculated from daily minima and maxima. *Agricultural and Forest Meteorology* **46** (3): 193–209 DOI: 10.1016/0168-1923(89)90064-6

Rivera A, Acuña C, Casassa G, Bown F. 2002. Use of remotely sensed and field data to estimate the contribution of Chilean glaciers to eustatic sea-level rise. *Annals of Glaciology* **34** (1): 367–372 DOI: 10.3189/172756402781817734

Rodriguez M, Ohlanders N, Pellicciotti F, Williams MW, McPhee J. 2016. Estimating runoff from a glacierized catchment using natural tracers in the semi-arid Andes cordillera. *Hydrological Processes* **30** (20): 3609–3626 DOI: 10.1002/hyp.10973

Rounce DR, McKinney DC. 2014. Debris thickness of glaciers in the Everest Area (Nepal Himalaya) derived from satellite imagery using a nonlinear energy balance model. *The Cryosphere* **8** (1): 1317–1329 DOI: 10.5194/tcd-8-887-2014

Rowan A V., Egholm DL, Quincey DJ, Glasser NF. 2015. Modelling the feedbacks between

mass balance, ice flow and debris transport to predict the response to climate change of debris-covered glaciers in the Himalaya. *Earth and Planetary Science Letters* **430**: 427–438 DOI: 10.1016/j.epsl.2015.09.004

Schauwecker S, Rohrer M, Huggel C, Kulkarni A, Ramanathan A, Salzmann N, Stoffel M, Brock B. 2015. Remotely sensed debris thickness mapping of Bara Shigri Glacier, Indian Himalayas. *Journal 0f Glaciology* **61** (228): 1–26 DOI: 10.3189/2015JoG14J102

Seibert J, Vis MJP, Kohn I, Weiler M, Stahl K. 2017. Technical Note: Representing glacier dynamics in a semi-distributed hydrological model. *Hydrology and Earth System Sciences Discussions* (March): 1–20 DOI: 10.5194/hess-2017-158

Steiner JF, Pellicciotti F, Buri P, Miles ES, Immerzeel WW, Reid TD. 2015. Modelling ice-cliff backwasting on a debris-covered glacier in the Nepalese Himalaya. *Journal of Glaciology* **61** (229): 889–907 DOI: 10.3189/2015JoG14J194

Vicuña S, Garreaud RD, McPhee J. 2010. Climate change impacts on the hydrology of a snowmelt driven basin in semiarid Chile. *Climatic Change* **105** (3–4): 469–488 DOI: 10.1007/s10584-010-9888-4

Vijay S, Braun M. 2016. Elevation Change Rates of Glaciers in the Lahaul-Spiti (Western Himalaya, India) during 2000–2012 and 2012–2013. Remote Sens. 8, 1038.

Vincent C, Wagnon P, Shea JM, Immerzeel WW, Kraaijenbrink P, Shrestha D, Soruco A, Arnaud Y, Brun F, Berthier E, et al. 2016. Reduced melt on debris-covered glaciers: Investigations from Changri Nup Glacier, Nepal. *Cryosphere* **10** (4): 1845–1858 DOI: 10.5194/tc-10-1845-2016

Watson CS, Quincey DJ, Carrivick JL, Smith MW, Rowan A V, Richardson R. 2018. Heterogeneous water storage and thermal regime of supraglacial ponds on debris-

covered glaciers. *Earth Surface Processes and Landforms* **43** (1): 229–241 DOI: 10.1002/esp.4236

WGMS 2017. Global Glacier Change Bulletin No. 2 (2014–2015). Zemp, M., Nussbaumer, S. U., Gärtner-Roer, I., Huber, J., Machguth, H., Paul, F., and Hoelzle, M. (eds.), ICSU(WDS)/IUGG(IACS)/UNEP/UNESCO/WMO, World Glacier Monitoring Service, Zurich, Switzerland, 244 pp., doi:10.5904/wgms-fog-2017-10.

Willis MJ, Melkonian AK, Pritchard ME, Rivera A. 2012. Ice loss from the Southern Patagonian Ice Field, South America, between 2000 and 2012. *Geophysical Research Letters* **39** (17): 1–6 DOI: 10.1029/2012GL053136

Table 1: Characteristics of the automatic weather stations (AWS) used in the study together with the variable recorded (T: temperature and P: precipitation) and the period of record.

AWS Map naming	Name	Location	Elevation [m asl]	Variable used	Period of record
YE	Yeso Embalse	33.68S, 70.09 W	2475	Daily T (Max and Min P	1999-2015
LN	Laguna Negra	33.66 S, 70.11 W	2780	T (Daily max and min ; hourly)	2013-2015
B-on	Bello on-glacier	33.53 S, 69.93 W	4134	T (Hourly)	11/2013-04/2014 10/2014-6/2015
Y-on	Yeso on-glacier	33.52 S, 69.92 W	4428	T (Hourly)	11/2013-04/2014 11/2014-04/2015
Y-off	Yeso off glacier	33.53 S, 69.92 W	4300	T (Hourly)	11/2013-04/2014
PI13	Piramide on-glacier	33.57 S, 69.89 W	3655	T (Hourly)	11/2013-04/2014
PI14	Piramide on-glacier	33.59 S, 69,89 W	3494	T (Hourly)	04/2014-10/2015
PI-off	Piramide off glacier	33.61 S, 69,91 W	3020	T (Hourly)	05/2014-04/2015

Table 2: Automatic weather stations (AWSs) and respective years used for the calculation of the air temperature lapse rates

Month	**AWSs and Year**	**Valid days per year**
January	Yeso Embalse (2014-2015)- Piramide off (2015)- Yeso off (2014)	31 days each year
February	Yeso Embalse (2014-2015)- Piramide off (2015)- Yeso off (2014)	28 days each
March	Yeso Embalse (2014) - Yeso off (2014)	13 days
April	Yeso Embalse (2014) -Piramide on (2014)	12 days
May	Yeso Embalse (2014) - Piramide on (2014)	31 days
June	Yeso Embalse (2014) - Piramide on (2014)	30 days
July	Yeso Embalse (2014-2015)-Piramide on (2014-2015)	31 days each year
August	Yeso Embalse (2014-2015)-Piramide on (2014-2015)	31 days each year
September	Yeso Embalse (2014-2015)-Piramide on (2014-2015)	30 days each year
October	Yeso Embalse (2014-2015)-Piramide on (2014-2015)	31 days
November	Yeso Embalse (2013-2014)- Piramide off (2014)- Yeso off (2013)	25 days for 2014 and 15 days 2013
December	Yeso Embalse (2013)- Yeso off (2013))	31 days

Table 3: Geodetic surface elevation change rate in the periods 2000-2013 and 2013-2015 for the three study glaciers.

Glacier	**Δh 2000-2013**	**Δh 2013-2015**
Bello	-0.01 ± 0.09 **[m year^{-1}]** -0.15 ± 1.23 **[m]**	-1.15 ± 0.15 **[m year^{-1}]** -2.31±0.30 **[m]**
Yeso	-0.03 ± 0.09**[m year^{-1}]** -0.43 ± 1.23 **[m]**	-1.08 ± 0.15**[m year^{-1}]** -2.17 ± 0.30**[m]**
Piramide	-0.14 ± 0.09**[m year^{-1}]** -1.88 ± 1.23**[m]**	-0.75 ± 0.15**[m year^{-1}]** -1.50 ± 0.30**[m]**

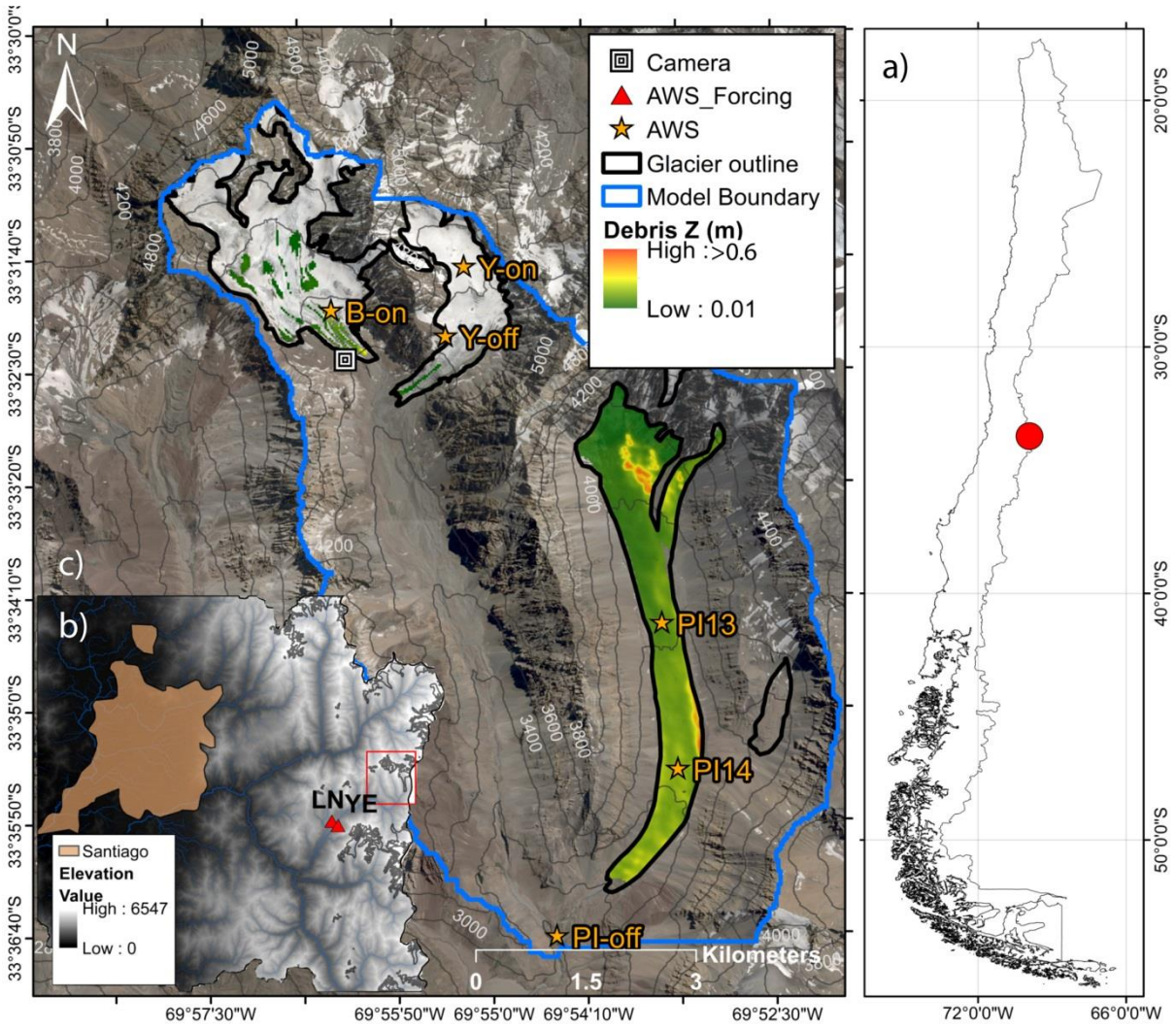

Figure 1. (a) Location of the study area in Chile, (b) location of the catchment (red box), near Santiago and c) map of the Rio del Yeso catchment including the study glaciers, the local automatic weather stations (AWS) and the estimated debris thickness map. The locations of Yeso Embalse (YE) and Laguna Negra (LN) weather stations are shown in (b).

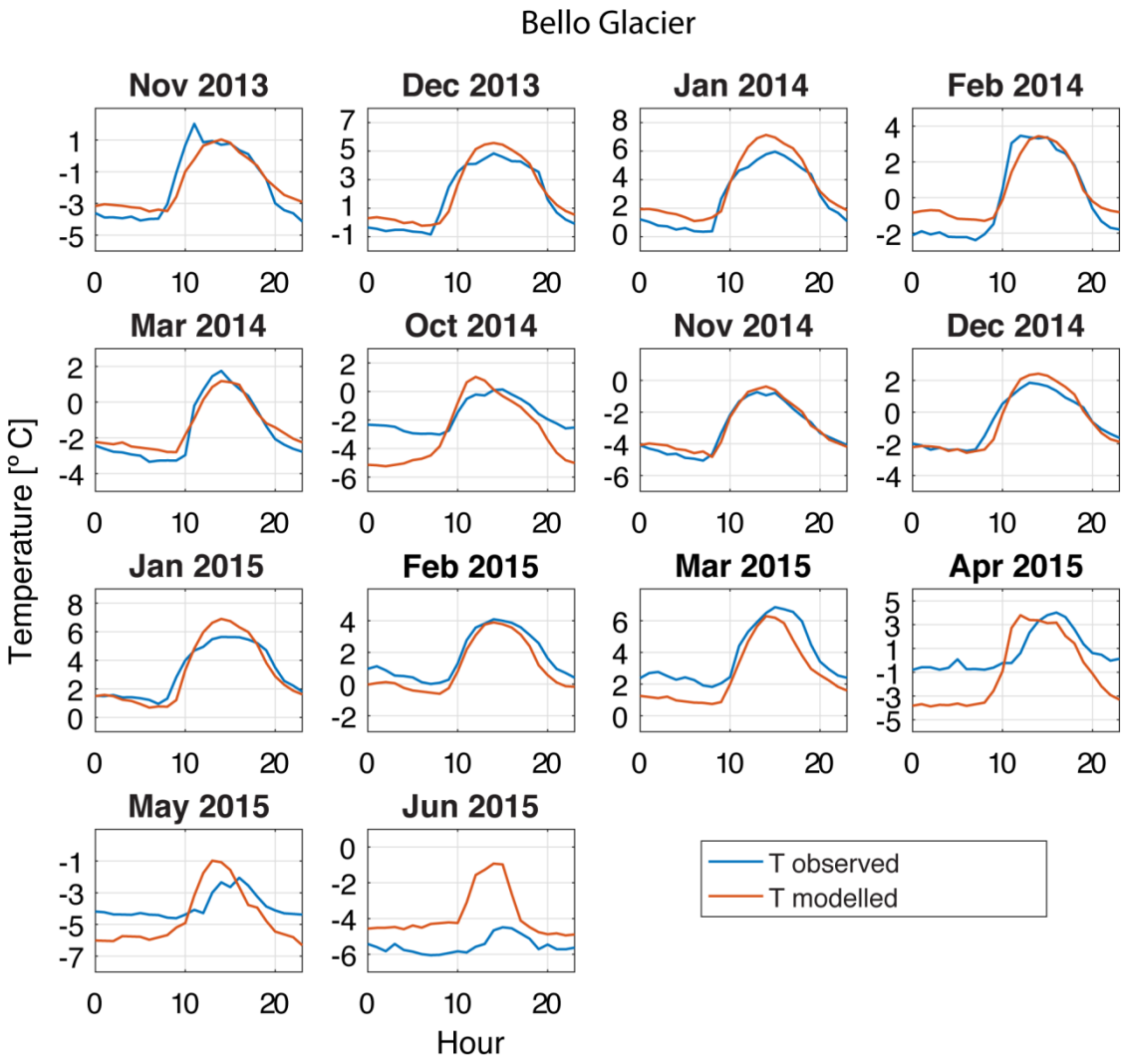

Figure 2: Validation of the air temperature extrapolation method on Bello Glacier (Section 3.2): comparison of observed (blue) and modelled (red) average hourly temperature at Bello Glacier AWS for each month, November 2013-June 2015.

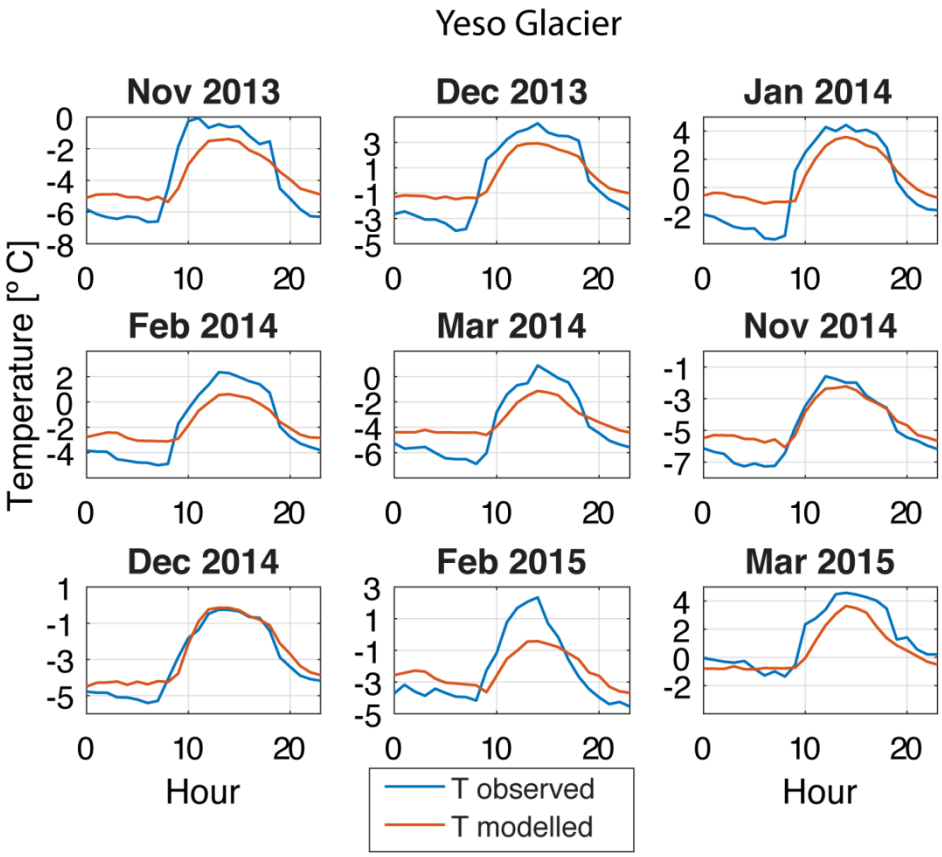

Figure 3: Validation of the air temperature extrapolation method on Yeso Glacier: comparison of observed (blue) and modelled (red) average hourly temperature at Yeso Glacier AWS for selected months between November 2013 and March 2015. Only months with data available at the Yeso Glacier AWS are shown.

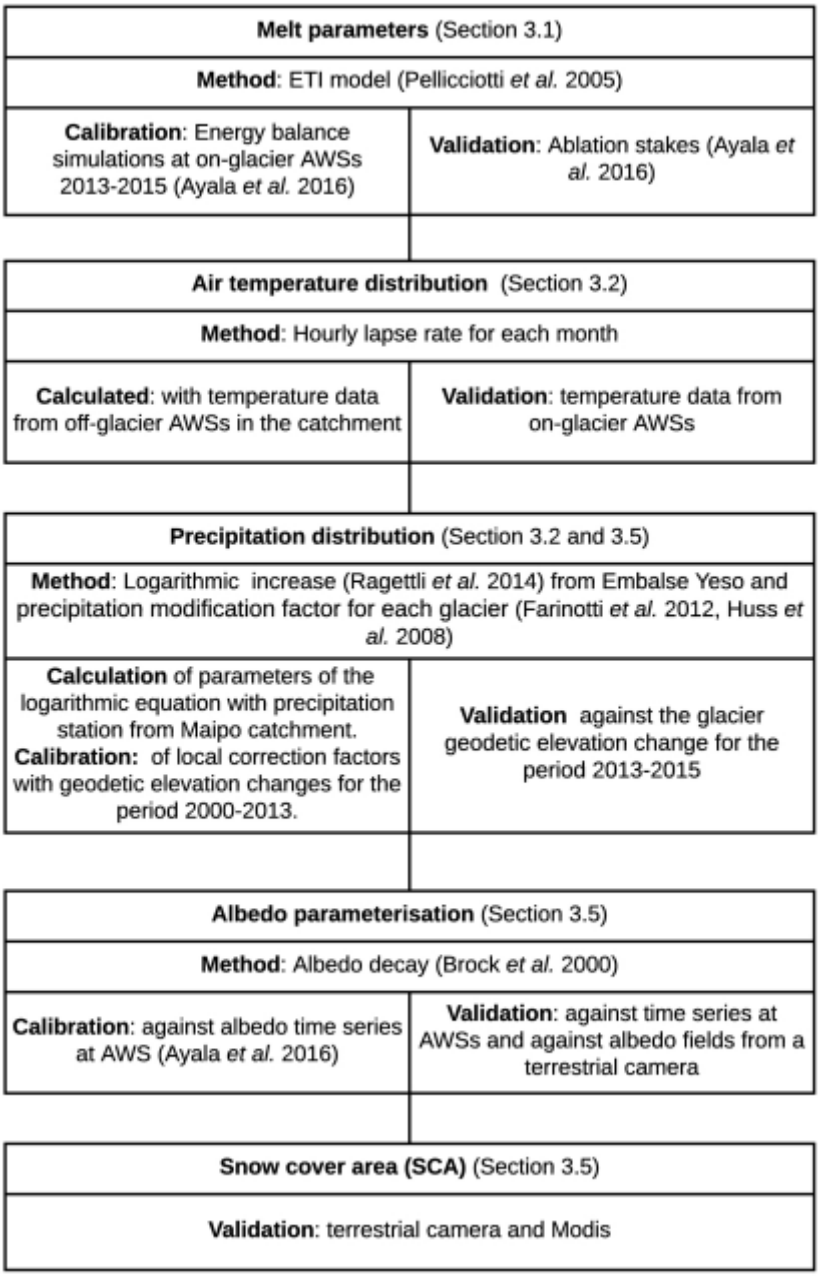

Figure 4: Scheme of the calibration and validation approach used in this study together with the datasets used in each step.

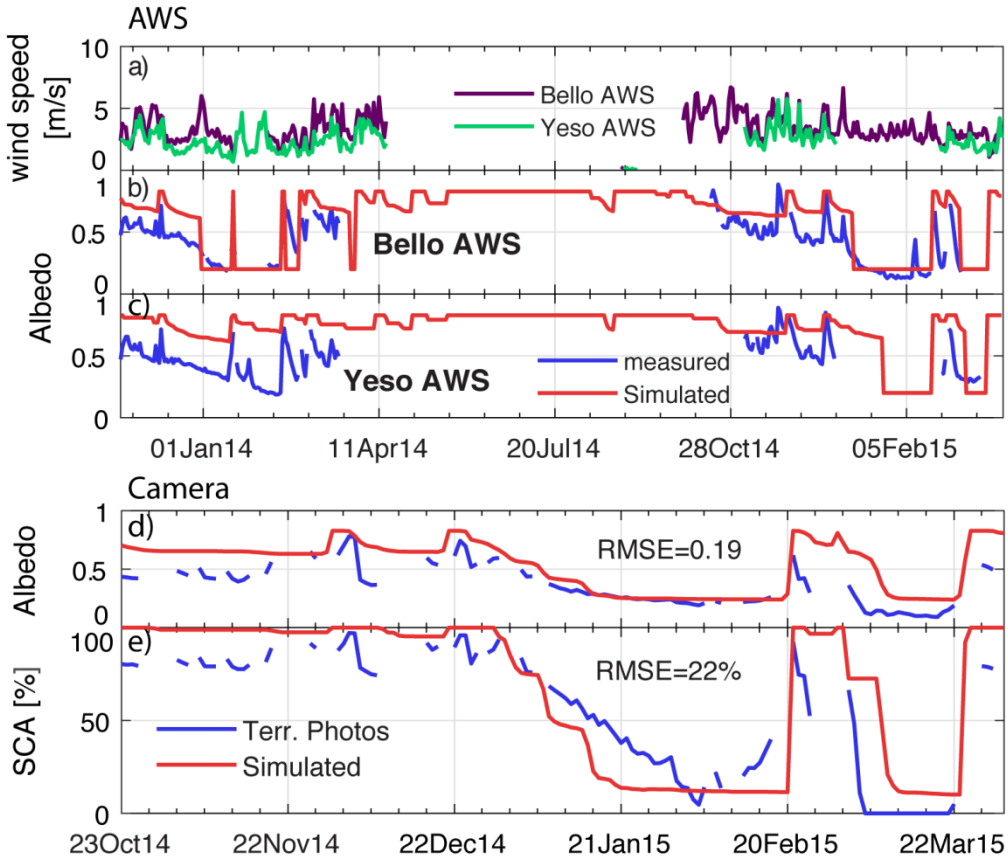

Figure 5: (a) Wind speed measured at Bello and Yeso automatic weather stations (AWS) during the period Jan 2014 to Feb 2015 (b and c) Comparison of observed and modelled daily albedo at the point-scale of the AWS on Bello and Yeso glaciers during the period Jan 2014 to Feb 2015. (d and e) Comparison of observed (from a terrestrial camera) and simulated distributed albedo and snow covered area on a portion of Bello Glacier (see Figure 1 and Section 3.5) covering an area of 0.84 km2, during the period Oct 2014 to March 2015. Note the different x-axis scale of the lower two panels.

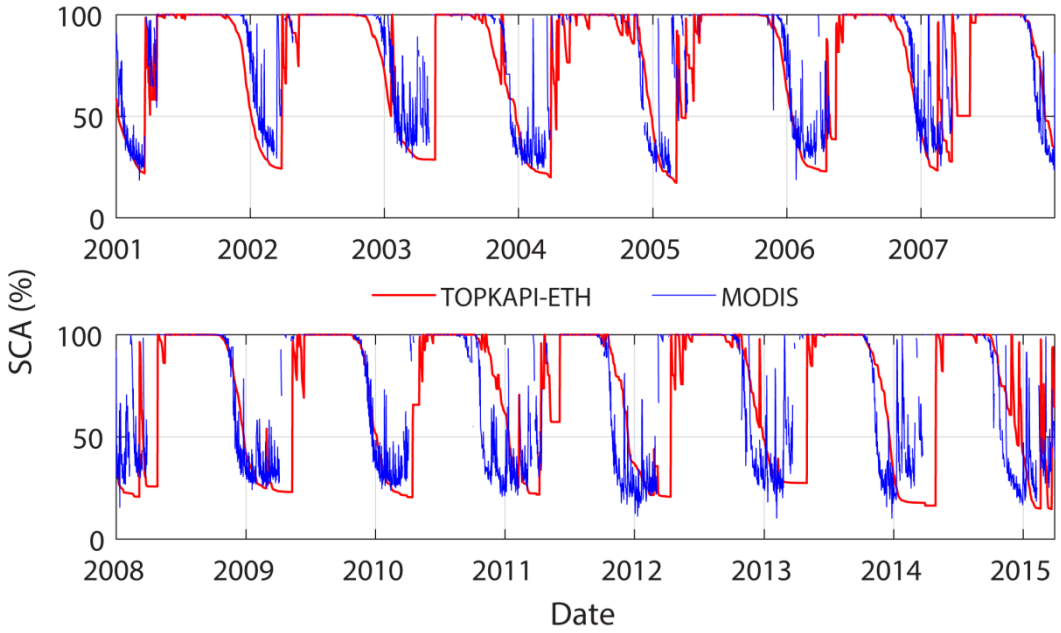

Figure 6: Comparison of the modelled TOPKAPI-ETH snow cover area (SCA) for the period 2001-2015 and MODIS MOD10A1 SCA. The MODIS SCA is provided as a catchment-wide average after filtering of clouds (see text).

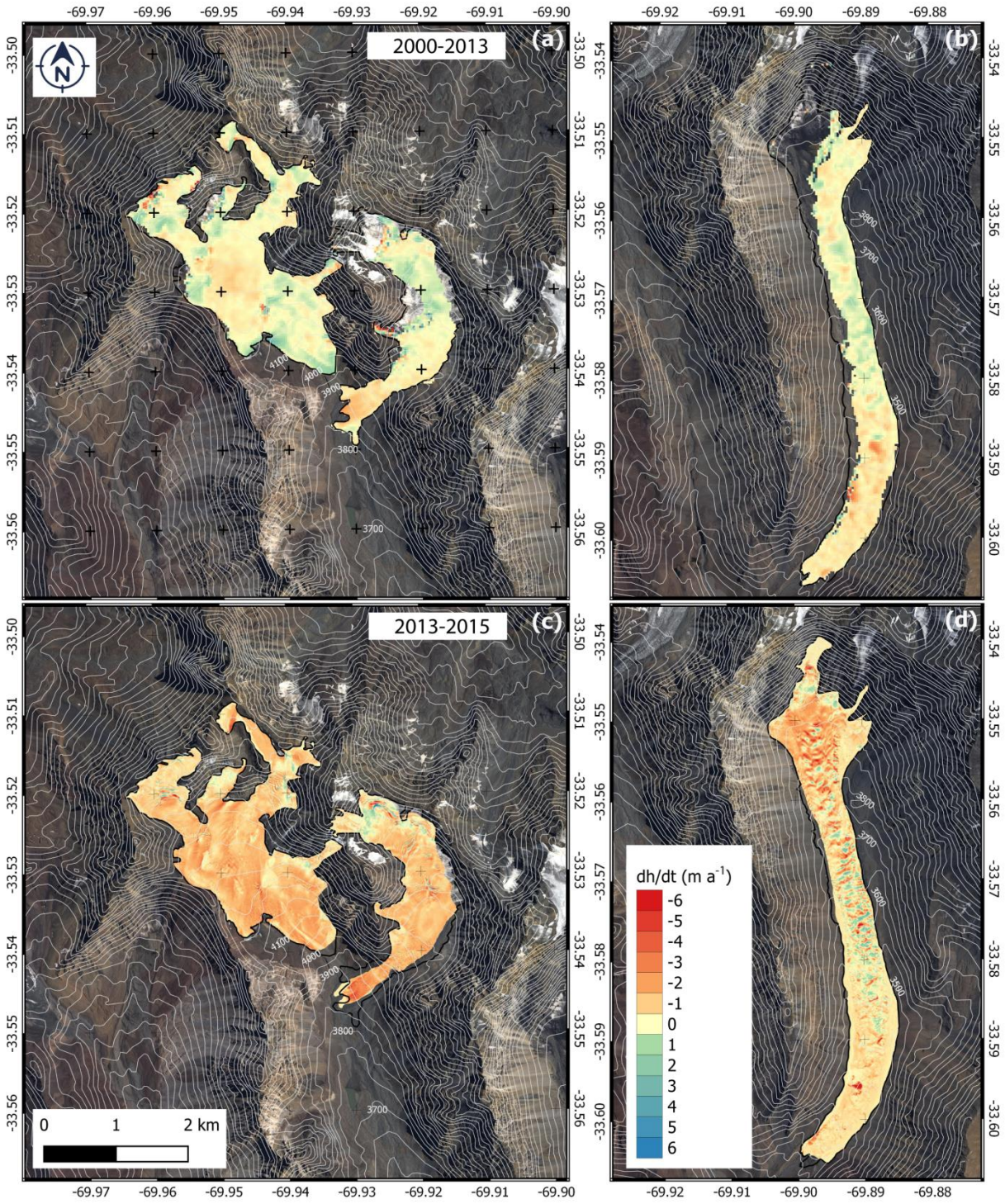

Figure 7: Geodetic elevation changes (Section 3.4) for the periods 2000-2013 (from SRTM and TanDEM-X DEMs)) (a and b) and 2013-2015 (c and d) (from the Lidar DEMs). For both periods, Bello and Yeso glaciers are shown on the left panels (a and c) and Piramide Glacier on the right (b and d).

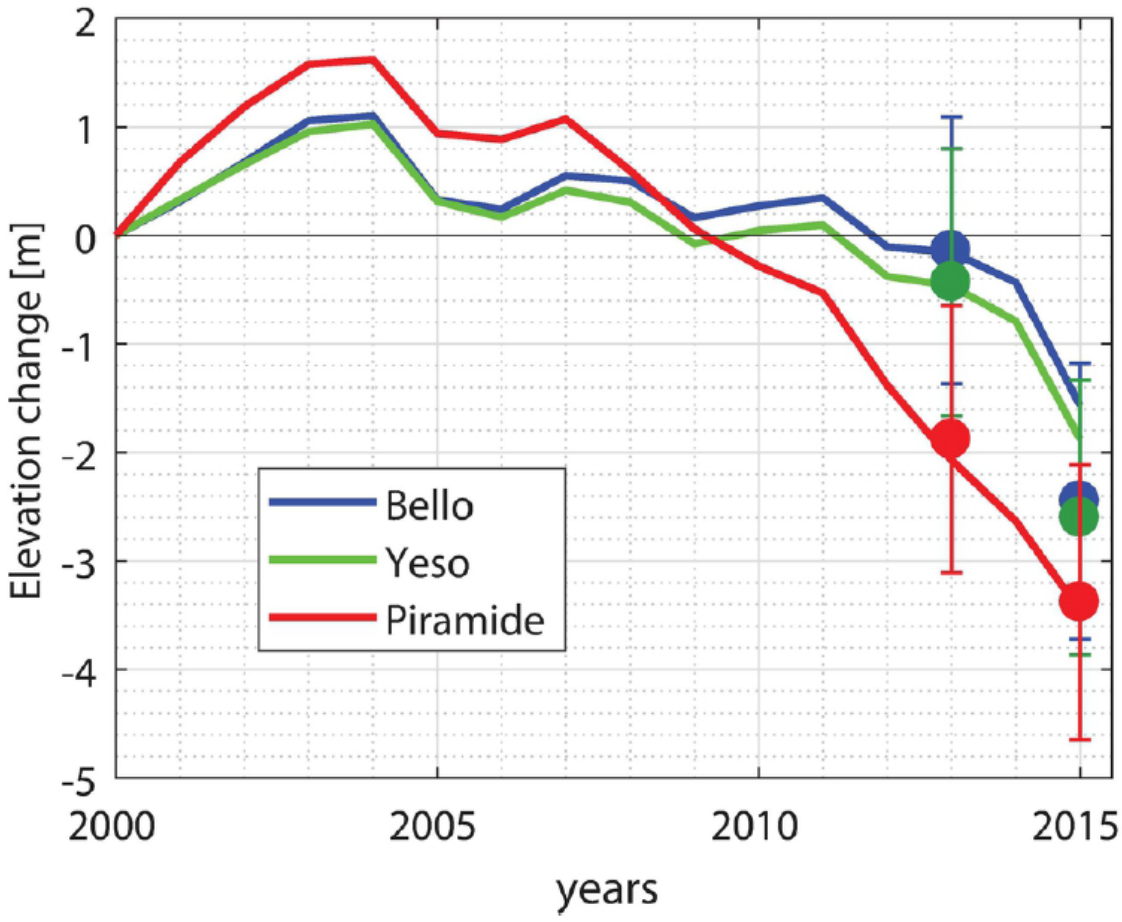

Figure 8: Cumulative elevation changes for the three study glaciers as simulated by TOPKAPI-ETH for the period 2000-2015 (colour lines). Dots in 2013 indicate the geodetic elevation change between 2000-2013 derived from differencing the SRTM and TanDEM-X DEMs, and used for calibration of the precipitation correction factors. Dots in 2015 show the geodetic elevation change for the period 2000-2015 (obtained from the sum of the elevation difference for the first period 2000 to 2013 and that of the second period 2013-2015 from differencing of the Lidar DEMs).

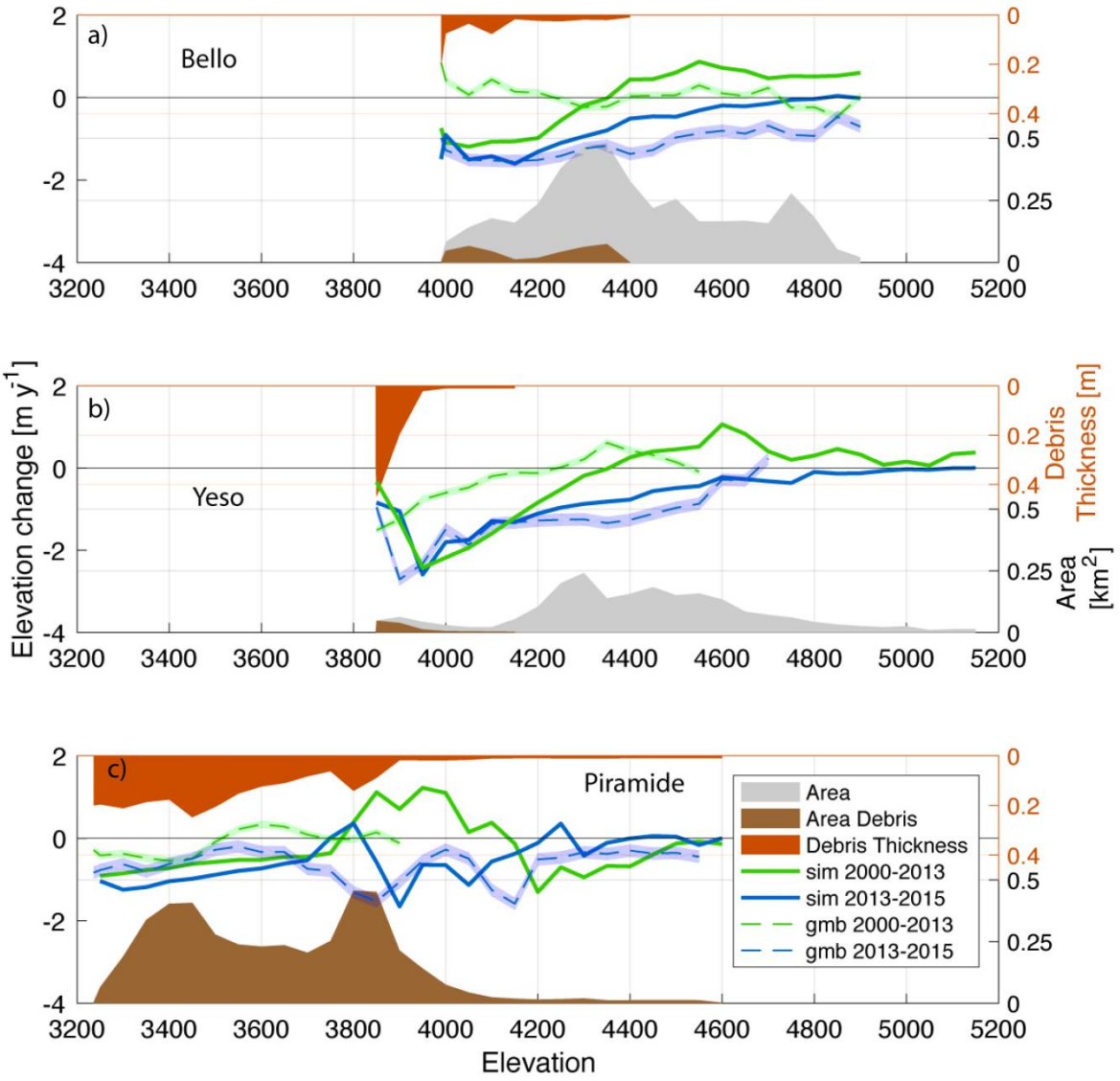

Figure 9: Simulated average elevation changes for 100 m elevation bands, and debris free (light grey) and debris-covered (brown) areas on (a) Bello, (b) Yeso and (c) Piramide glaciers. Average debris thickness for each elevation band is shown on the upper right axis. Simulated elevation changes in the periods 2000-2013 and 2013-2015 are shown by the green and blue continuous lines, respectively. Geodetic elevation differences are shown by the green and blue segmented lines in the period 2000-2013 and 2013-1015, respectively. Incomplete lines for the geodetic elevation change profiles are due to missing pixels in the corresponding elevation band.

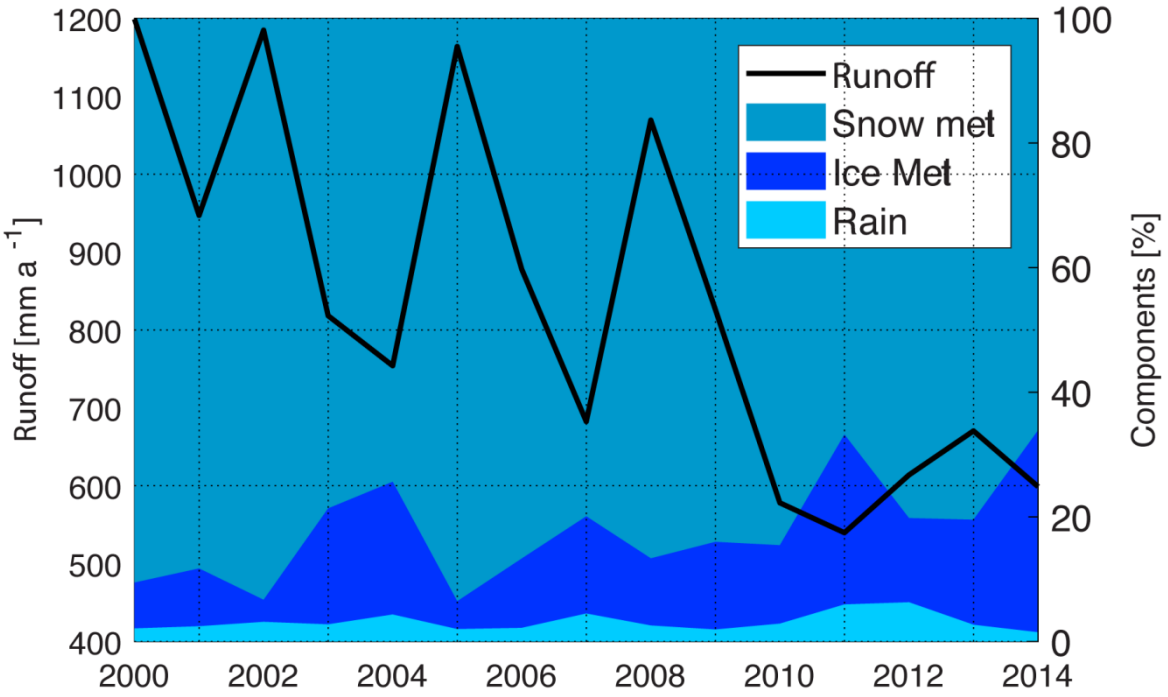

Figure 10: Annual average catchment runoff (left axis) and relative contribution (right axis) from snowmelt, ice melt and rain.

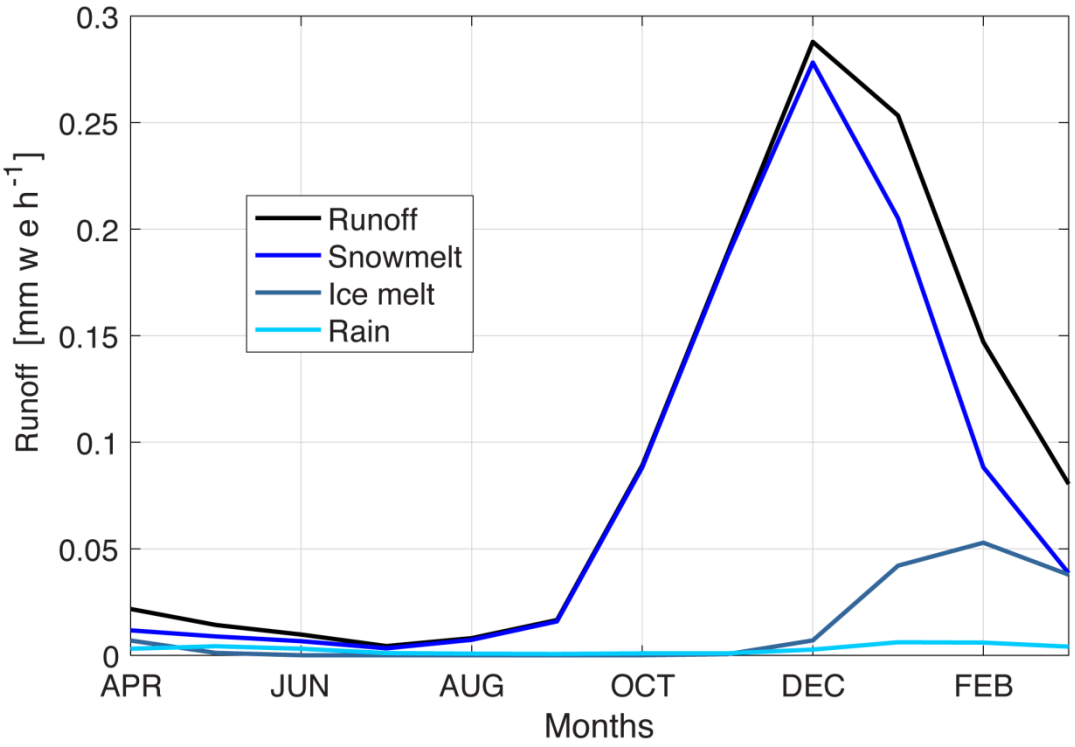

Figure 11: Monthly averages of simulated total runoff and runoff components (snowmelt, icemelt and rain) over the study period (2000-2015).

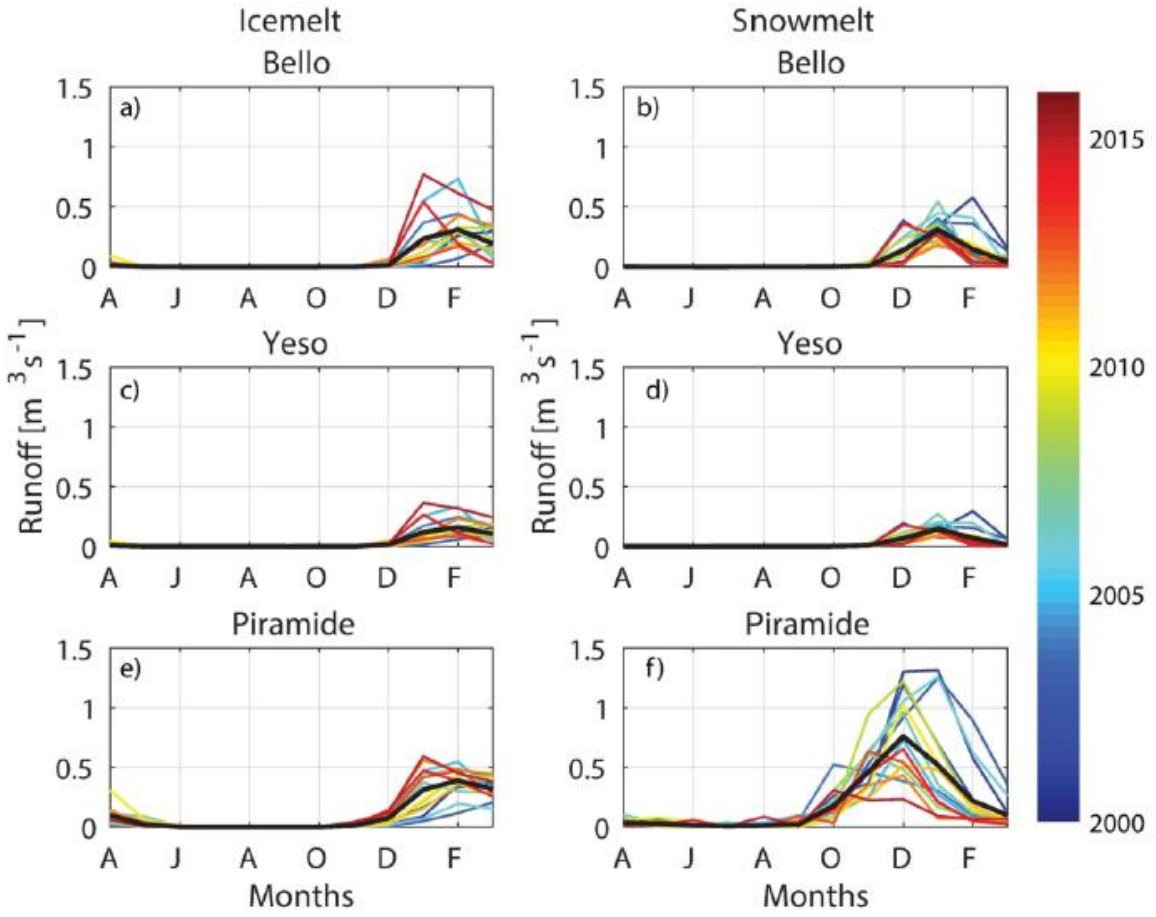

Figure 12: Monthly mean runoff generated by ice melt (left panels) and snowmelt (right panels) from (a-b) Bello, (c-d) Yeso and (e-f) Piramide glaciers. Each thin colour line represents an individual year (indicated by the colour bar). The average for the entire period (2000-2015) is shown as a bold black line.

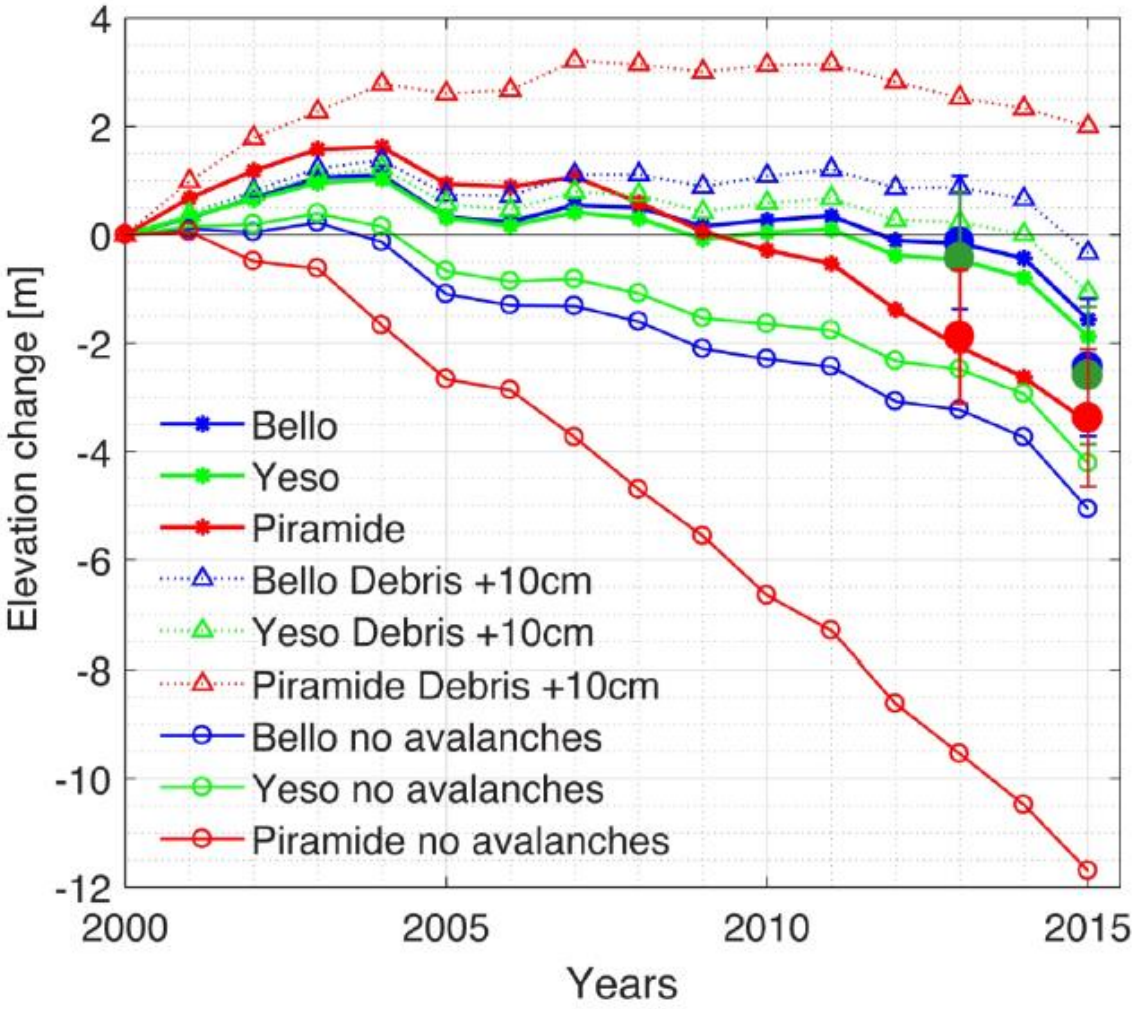

Figure 13: Comparison of modelled and observed (geodetic) elevation changes for additional model runs from a sensitivity analyses for the three glaciers: i) considering an additional 10 cm of supraglacial debris (triangles); and ii) ignoring the avalanching in the TOPKAPI simulations (hollow circles). The reference model (filled markers) and geodetic surface changes (large filled circles and error bars) are shown for comparison.